View metadata, citation and similar papers at core.ac.uk

brought to you by CORE

provided by Clemson University: TigerPrints

Clemson University
TigerPrints

All Theses | Theses

12-2012

ESTIMATING WATER FLUX AND STORAGE USING DISPLACEMENT MEASUREMENTS IN SAPROLITE AT DEPTH

Clay Freeman
Clemson University, clayfree@comcast.net

Follow this and additional works at: https://tigerprints.clemson.edu/all_theses

 Part of the Engineering Commons

Recommended Citation
Freeman, Clay, "ESTIMATING WATER FLUX AND STORAGE USING DISPLACEMENT MEASUREMENTS IN SAPROLITE AT DEPTH" (2012). *All Theses*. 2239.
https://tigerprints.clemson.edu/all_theses/2239

This Thesis is brought to you for free and open access by the Theses at TigerPrints. It has been accepted for inclusion in All Theses by an authorized administrator of TigerPrints. For more information, please contact kokeefe@clemson.edu.

ESTIMATING WATER FLUX AND STORAGE USING DISPLACEMENT MEASUREMENTS IN SAPROLITE AT DEPTH

A Thesis
Presented to
the Graduate School of
Clemson University

In Partial Fulfillment
of the Requirements for the Degree
Master of Science
Environmental Engineering

---

by
Clay Freeman
December 2012

Accepted by:
Dr. Lawrence C. Murdoch, Committee Chair
Dr. Ronald Falta
Dr. Nadarajah Ravichandran

ABSTRACT

Water storage in the soil is important for many hydrologic problems, but measuring how the storage changes at an appropriate scale remains a challenge. The objective of this thesis is to evaluate the feasibility of estimating change in water content in soil by measuring vertical displacement in underlying soils. This approach is appealing because the averaging volume of the displacement scales with the depth at which the measurements are taken. This should result in measurements of changes in soil moisture that are averaged over regions 10s to 100s of meters across, a measurement scale that is much larger than that of commercially available moisture sensors and that would be useful for model calibration and other applications.

The approach of this research is to develop an instrument for measuring displacement and to evaluate the instrument in a field setting by monitoring displacement along with environmental variables. The instrument developed for this work is called a *Sand Extensometer*, or Sand-X, and it is designed for applications in sand or other unlithified materials. The Sand-X was evaluated in three installations at two field sites in the vicinity of Clemson, SC. One instrument was installed at 2 m and two were installed at 6 m depths in saprolite above the water table.

The Sand-X was sensitive to precipitation events during continual sampling at 1-minute intervals for months, and periods between precipitation events indicated behavior suggestive of decreasing soil moisture. Increases in soil moisture due to typical precipitation events of 10 – 15 mm corresponded to displacements of about 1 micron of compression. The soil expanded at a typical rate of 0.5 μm da^{-1} between precipitation

events. This expansion was interpreted as unloading of the soil due to decrease in soil moisture.

The 6-m-deep installations were calibrated using precipitation events greater than 5 mm. The average response of one instrument was -0.16 μm displacement mm^{-1} rainfall with an R^2 of 0.95 for one instrument and -0.66 μm displacement mm^{-1} rainfall with an R^2 of 0.54 for another instrument. Using these calibrations, the periods between precipitation events were interpreted as periods of soil drying resulting from the combined effects of evapotranspiration and recharge. The net evapotranspiration and recharge estimated from land pan measurements and hydrograph data respectively was 43 cm with a standard deviation of 14.9 cm, and the net soil water loss estimated from displacement measurements was 27 cm with a 95% confidence interval of ±6.7 cm. These results indicate that the measurements of water loss from displacement are consistent with independent estimates of water loss.

All of the installations were sensitive to fluctuations in barometric pressure. Typical diurnal pressure changes of about 400 Pa correspond to displacements on the order of 1 micron at depth. These effects were reduced slightly using an analytical solution for the soil response to barometric loading.

DEDICATION

This work represents an effort that would have been too great for me to overcome alone. I wish to dedicate this work to my closest friends and family who have helped and encouraged me to finish strong. I dedicate this work to you, mom and dad, who have balanced perfectly the space you have given me to succeed with the security you have given me against life's hiccups. I dedicate this work to you, m and d, who motivated me to become mature early in life and who have prevented me from becoming too serious in graduate school. And I dedicate this work to you, *kochanie*, for being a constant source of distraction that has given me a sense of peace and sanity.

ACKNOWLEDGEMENTS

I would like to thank Leonid Germanovich for his perseverance and patience. He has been instrumental in demonstrating the potential of this work. I would also like to thank the Clemson University Geology creative inquirists. I hope that the time they spent learning from this project was as beneficial to them as their work and friendships have been to me.

I would like to express my utmost gratitude to my advisor, Larry Murdoch. His ideas, suggestions, time, patience, and understanding were the foundation for the success of this work. More importantly, I am grateful for the excitement and curiosity he has given me for the pursuit of science.

This work was funded by the National Science Foundation, Project 0944315.

TABLE OF CONTENTS

Page

Table of Contents (Continued)

Page

LIST OF TABLES

Table Page

LIST OF FIGURES

Figure Page

List of Figures (Continued)

Figure Page

CHAPTER 1: INTRODUCTION

Water storage in soil is important to a fundamental and applied understanding of hydrologic systems, but few technologies are capable of measuring changes in water storage between the 10^{-2}-m-scale of in-situ sensors (Parsons and Bandaranayake, 2009) and the 10^{4}-m-scale of satellite sensors (Entekhabi *et al*., 2004). This is important because applications related to watershed-scale processes (e.g. ecosystem dynamics (Hwang *et al*., 2009; Marks *et al*. 1993; Palmer *et al*., 2009; Iwata *et al*., 2010), agriculture (Bastiaanssen *et al*., 2000), flood prediction (Bell *et al*., 2009; Yatheendradas *et al*., 2008), water management (Dolph *et al*., 1991; Marks *et al*., 1993; Lettenmaier *et al*., 1992), watershed response (Markstrom *et al*., 2011; Bjerklie *et al*., 2011) etc.) can be sensitive to variations in water storage at scales between 10^{2} m and 10^{3}m (e.g. Thoma *et al*., 2008; Robinson *et al*., 2008), which spans the gap in measurement scales of readily available technologies. Many in-situ sensors can be required to characterize water storage change at these scales (Famiglietti *et al*., 2008), and current satellite data can be too coarse to provide the spatial and temporal resolution needed for many applications.

Numerical models used to understand watershed-scale processes are often set up with grid blocks or elements in this same scale gap (e.g. Sulis *et al*., 2011; Hsu *et al.*, 2012, Crow *et al*., 2005), so the data needed to calibrate soil moisture change at the grid block scale are commonly unavailable. Selecting a grid scale that provides the desired resolution and accuracy and that can be paired with hydrologic measurements at a similar scale is not a trivial task (Artan *et al*., 2000; Robinson *et al*., 2008; Famiglietti *et al*.,

2008). Variation in soil moisture measurement increases with the scale of measurement (Western and Blöschl, 1999) and changes with the mean soil moisture of the cell (Famiglietti *et al*., 2008) such that the number of samples required to estimate the mean increases with the scale of the estimate (Brocca *et al*., 2010; Famiglietti *et al*., 2008). In practice, collecting sufficient measurements to guarantee reasonable accuracy is rarely done (Famiglietti *et al*., 2008), and even large soil moisture data networks often provide on average only one *in situ* observation point within the footprint of satellite-based soil moisture measurements (Crow *et al*., 2005).

Efforts are being made to span the measurement scale information gap through detailed studies of variability in soil moisture and the factors that affect the variability (Brocca *et al*., 2010; Famiglietti *et al*., 2008; Western and Blöschl, 1999); understanding the impact of model grid size and optimizing the grid for input measurements (Artan *et al*., 2000; Sulis *et al*., 2011); and developing new technology or improvements to old technology (Robinson *et al*., 2008). Although it is possible to optimize numerical model grids to balance output accuracy with the computational demand (Artan *et al*., 2000), improvements to the model do not eliminate the need for representativeness of the measurement scale. The COsmic-ray Soil Moisture Observing System (COSMOS), which measures neutron emission from above the ground surface, averages soil moisture at the scale of 10^2 m to a depth of 15 to 70 cm and is sensitive to water storage above the soil, for example in the form of snow or intercepted water (Shuttleworth *et al*., 2010). Methods for estimating soil moisture using electromagnetic radiation measurements such as radiometers (Kerr, 1998), radar (Kurum *et al*., 2009), and LiDAR (Tenenbaum *et al*.,

2006) may be ground-based (Lemaître *et al*., 2004), airborne (Delwart *et al*., 2008; Saleh *et al*., 2009), or spaceborne (Entekhabi *et al*., 2004) and yield measurements over regions ranging from 10^{-1} m (Korpela *et al*., 2009) to 10^{4} m (Kurum *et al*., 2009) that scale with the height, angle of incidence, and frequency range of the measurement (Korpela *et al*., 2009; Gupta *et al*., 2011). These methods must be calibrated to the surface roughness of the site (Njoku and Entekhabi, 1996; Delahaye, 2002).

A technique exists that is capable of estimating soil moisture both near the surface and at depth across this measurement scale gap using the response of pore pressure in a thick clay layer (van der Kamp and Maathius, 1991; Bardsley and Campbell, 1994). The change in soil moisture is deduced by measuring the effect on pore pressure of the corresponding load change on the soil (van der Kamp and Maathius, 1991). This method offers the advantage of making measurements over an averaging volume that scales with the depth of the measurement, but it is limited by the availability of suitable geologic formations (van der Kamp and Schmidt, 1997).

Purpose

The goal of this research is to evaluate the feasibility of using measurements of vertical displacements of soil at depth to infer changes in loads caused by hydrologic processes. Technology that is capable of resolving small displacements of soil at depth may be used to make measurements of changes in load at the surface averaged over an area that scales with the depth of the displacement measurement. Though such a technique would not be the only solution available to measuring soil moisture at the intermediate scale, it would be complementary to other techniques and could enable the

inference of the near-surface fluxes. This type of technology may also be applicable to a variety of non-hydrologic studies as well.

Objective

The hypothesis is that hydrologic processes near the ground surface such as fluctuations in soil water content cause measurable displacements at depth that can be used to characterize the behavior of the system. The objective of this research is to test this hypothesis by making the necessary measurements and comparing them to weather measurements.

Approach

The general approach was to develop a device to measure soil displacement, test the device at the lab scale, and install the working design in the field to evaluate its performance in a natural setting. Experiments were performed to provide insight into specific components of the device and to inform the design iteration process. Field experiments and observations incorporated as many concurrent measurements as were necessary and practical to observe correlation between hydrologic events such as precipitation and the resulting displacement.

Current Technologies

Methods used to measure the near surface soil moisture may be direct, *in situ* techniques (Parsons and Bandaranayake, 2009; van der Kamp and Schmidt, 1997), direct, *ex situ* (e.g. geophysical and remote sensing) techniques (Robinson *et al*., 2008), or indirect techniques such as performing a water balance (Thornthwaite, 1948). Promising

in situ techniques that measure soil moisture at the scale of 10^2 to 10^3 m are limited to using pore pressure measurements in clay layers to estimate the load change on the soil. *Ex situ* techniques have been more successful at this scale with ground-based techniques such as ground penetrating radar (GPR) (Robinson *et al*., 2008), radiometry (Kerr, 1998), and neutron measurement (Shuttleworth *et al*., 2010).

Ground penetrating radar is a non-invasive method for making estimates of soil moisture at the intermediate scale (Robinson *et al*., 2008). GPR works by transmitting high-frequency electromagnetic waves from one antenna and observing the time delay and magnitude of the return waves at a second antenna. This approach has been used in a number of studies to investigate the distribution of soil water (Galagedara *et al*., 2004) and can be used to determine the depth of the wetting front (Vellidis *et al*., 1990). The scale of these measurements range from meters to tens of meters (Robinson *et al*., 2008) with the vertical and horizontal scale of measurement dependent on the distance between the antennas (van Overmeeren *et al*., 1997; Grote *et al*., 2003). A drawback of GPR is that it produces datasets that require a great deal of technical skill to interpret accurately (Robinson *et al*., 2008).

Ground-based, passive, radiometers measure naturally-occurring electromagnetic emission, which can be correlated to the soil moisture (Saleh *et al*., 2009), within a target area and frequency range. The averaging region of radiometers is a function of the height and angle of incidence of the receiver (Gupta *et al*., 2011). Ground-based radiometers offer the advantage of being able to make measurements at high frequencies compared to satellite-based radiometers (Lemaître *et al*., 2004). Radiometers must be calibrated to the

temperature (Delahaye *et al*., 2002) and require baseline measurements for different plant cover (Saleh *et al*., 2007) and surface roughness (Gupta *et al*., 2011).

Measurement of neutrons emitted from the ground surface *ex situ* provides a means of measuring soil moisture (Kodama *et al*., 1985) and surface water storage over an area with diameter of approximately 660 m (Shuttleworth *et al*., 2010) and to a depth of 60 cm depending on the soil moisture (Desilets *et al*., 2010). As with ground-based radiometers, neutron measurement can be performed at high temporal resolution (Zreda *et al*., 2008). An advantage of this technique is that the neutron emission of the soil is largely insensitive to the type of soil, and the instrument only requires an initial soil moisture offset (Shuttleworth *et al*., 2010). The correlation between the neutron count and volumetric water content is nonlinear, and as a result, soils with relatively high water content require longer periods of time to achieve a specified level of uncertainty (e.g. approximately 4 hours to achieve 2% uncertainty for a measurement of 30% water content) than soils with relatively low soil moisture (Zreda *et al*., 2008).

The water balance method can be used to estimate soil moisture near the surface by taking the difference of measured or estimated water inflow and outflow. Some typical system fluxes include direct evaporation off of plants and from the soil, transpiration, runoff, recharge or potential recharge, and precipitation (Ruiz *et al*., 2010). This approach gives the user the flexibility of estimating the fluxes through the vadose zone rather than the soil moisture (Malek and Bingham, 1993; Ruiz *et al*., 2010). Measuring the fluxes presents a considerable challenge in terms of the representativity (Andréassian *et al*., 2004) in addition to the physical aspects of measurement error (Legates and Willmott,

1990). Further, the pursuit of accuracy in model results can introduce unnecessary prediction uncertainty and model complexity (Atkinson *et al*., 2002).

Application

A major hydrologic application of displacement measurements at depth would be the measurement of soil moisture change and inference of surface fluxes averaged on the plot to regional scale. Soil moisture change can be measured using displacement at depth that is calibrated to known changes in soil water at the surface from measurements of precipitation, ET, and soil moisture. Further, by pairing displacement with near-surface soil moisture measurements averaged over the same area, it may be possible to separate the components of a water balance of the vadose zone. This is important because these fluxes, if they are measured at all, are often unrepresentative of the application (Sharma, 1986; Bohnenstengel *et al*., 2011; Cooper *et al.* 2011).

Displacement measurements may be used to characterize processes of subsidence under conditions of aquifer loading and dewatering (e.g. Kihm *et al*., 2007; Kim, 2000). Subsidence has long been observed as resulting from draining large stores of water from the ground (Galloway *et al*., 1999), and with growing concerns due to drought conditions, which are significant enough to begin affecting food prices and availability, and extreme overuse of groundwater (Barnett *et al*., 2005; Dennehy, 2002), a good understanding of the effect subsidence has on the storage capacity of dewatered aquifers has become important. Measurements of soil strain in an aquifer provides a foundation for studying the subsidence process as it occurs, and distributed measurements through the aquifer

column can be used to identify layers prone to collapse during de-watering (Wisely and Schmidt, 2010).

Similarly, it may be possible to measure the changes in water mass that occur during freeze-melt cycles of glaciers and snow pack. In particular, glacial movement is significant enough to induce flow in the mantle (Farrell, 1972), suggesting that its influence on soil deformation is similarly substantial. This could provide insight into management of frozen-water resources as climate change threatens to redistribute fresh water (Barnett et al., 2005; Bates et al., 2008). The ability to measure change in water storage as snow accounting for variability would provide a means for improving estimates of the water budget, which is sensitive to the net accumulation of snow (Smerdon *et al.*, 2009).

It may be possible to partially characterize the *in situ* poroelastic system using measurements of displacement, weather, and pore pressure, offering insight into the *in situ* mechanical behavior of the soil matrix. A basic demonstration of this would be using concurrent measurements of precipitation events to correlate the soil deformation to a particular loading. This information could be used to estimate the effective modulus of the soil. Surface deformation data collected by InSAR has been used to estimate the storativity associated with the compressibility of the aquifer skeleton (Wisely and Schmidt, 2010). The elastic parameters of a hydrologic system are sensitive to the stress and saturation states (Bemer *et al*., 2004), suggesting that, especially under conditions of extreme changes in the system state (e.g. subsidence (Kim, 2005)), understanding how

and when these parameters change is critical for accurately modeling the behavior of the system.

The ability to measure changes in surface load would make a wide variety of non-hydrologic measurements possible. With sufficient considerations for the method of installation, it may be possible to observe changes in load due to leafing and forest fire, offering the possibility of making direct estimates of change in the carbon balance during these events. This would yield broad range of application for this method in climatological and ecological studies since current approaches for estimating the regional carbon balance depend heavily on statistical analyses because of the difficulty of making measurements for validation (Chen et al., 2000). Soil displacement measurements may also be used to observe settling for determining infrastructure stability during construction of buildings or dams (e.g. Anderson and LaFronz, 2007). It may be possible to program the device to measure high-frequency seismic activity when it occurs while simultaneously making low frequency, surface-load-based measurements. Additionally, with three sensors, it may be possible to track point loads at the surface. This device may be installed adjacent to highways without disturbing current infrastructure and used to measure road use and to weigh vehicles as they pass.

The Concept of Weighing Soil Moisture

One method that has been proposed to estimate large-scale, average changes in the moisture content is to measure water pressure change in a compressible clay aquitard (van der Kamp and Schmidt, 1997; Barr et al., 2000). A change in moisture content alters the load in the subsurface, and this changes the water pressure in the clay. When a load

change representing an increase or decrease in soil moisture content occurs, it is distributed between the soil matrix and the pore fluid. In an aquitard composed of a soft material, the majority of the load is supported by pore pressure (van der Kamp and Maathuis, 1991). This occurs where the bulk modulus of the soil is less than that of water. The soil matrix restricts the flow of water, and in horizontally extensive formations, only the change in vertical pressure gradient will affect the pore pressure measurement (van der Kamp and Schmidt, 1997; Barr et al., 2000). If the change in horizontal gradient is small compared to the vertical gradient, measurements of pressure head change will be representative of change in surface loading, but if it is large, vertical loading will no longer dominate the pore pressure signal and application of this method would require a detailed understanding of the background gradient (Barr et al., 2000).

This approach can resolve load changes over an area that is a function of the depth of the piezometer (van der Kamp and Schmidt, 1997; Davis and Selvadurai, 1996). An important result of the analysis by van der Kamp and Schmidt (1997) is that the pore pressure distribution that results from an infinite, uniform load will be spatially invariant. That is, a given change in distributed load will yield the same response in homogeneous soil independent of the depth of the measurement. This concept has been demonstrated with measurements of pressure changes taken at 300 m depth which correlated to loads caused by rainfall events, and it has been suggested that the signal may be observable at much greater depths (Sophocleous et al., 2006).

The pressure data from an aquitard is used to estimate changes in the soil moisture content by measuring and removing the effects of atmospheric pressure, earth tide

dilation, and background effects caused by fluctuations in the vertical change in pressure gradient (Barr et al., 2000). The change in pressure with time may be written as

$$\frac{\partial p}{\partial t} = \gamma\left(\frac{\partial p_a}{\partial t} + \frac{\partial p_e}{\partial t} + P + E + R\right) + D\frac{\partial^2 p}{\partial z^2} \quad (1)$$

where p is the pore pressure, γ is the loading efficiency, p_a is atmospheric pressure, p_e is the load resulting from earth tide dilation, P is the rate of precipitation, E is the rate of evapotranspiration, R is the rate of runoff, D is the hydraulic diffusivity, and z is the vertical coordinate (Barr et al., 2000). Atmospheric pressure and earth tide effects are both well-defined and can be removed from the signal readily, and if the soil is sandy, the runoff may be ignored (Barr et al., 2000). The magnitude of the vertical transient β is dependent on the permeability of the clay; as the permeability decreases, the β term diminishes and vice versa (Barr et al., 2000). In permeable or fractured clay units, this term must be estimated using background data during periods of no precipitation and minimal evaporation so it can be removed from the signal (Barr et al., 2000).

A similar method for estimating large-scale, average load changes makes use of pressure measurements from a confined aquifer (van der Kamp and Maathuis, 1991). In contrast with measuring the pore pressure in an aquitard, this approach is insensitive to vertical fluxes which would introduce error in pressure measurements, and it does not require the skill or effort to install and maintain that is required by wells installed in an aquitard (Marin et al., 2010). Further, because monitoring wells completed in confined aquifers are relatively common, this technique is widely applicable and can be performed on historical data (Marin et al., 2010).

For either of these methods to be practical, the effect of barometric pressure, which has a diurnal poroelastic effect on the soil, must be removed from the data (Bardsley and Campbell, 1994; Farrell, 1972). This requires the application of a site-specific analysis of the sensitivity of groundwater level to barometric pressure in order to isolate useful signal (Barr et al., 2000; Rojstaczer, 1988). This response, which includes the behavior of the unsaturated zone, is described by the barometric efficiency of the system, the pneumatic diffusivity of the unsaturated zone, the hydraulic diffusivity of the confining layer, and the permeability of the aquifer—all parameters that can be estimated or bounded with background barometric pressure and water level measurements (Rojstaczer, 1988). In addition to isolating data from the barometric effect, the barometric efficiency can be used to calculate the loading efficiency, thus acting as a calibration for these techniques (van der Kamp and Schmidt, 1997; Marin et al., 2010).

These methods provide a tool for observing changes in distributed soil moisture from both current and historical data sets, but both require specific geologic formations such as a clay layer or confined aquifer (van der Kamp and Schmidt, 1997). In this work, I investigate the concept of using solid strain measurements as an alternative to pore pressure measurements to estimate changes in water content at the surface. By using extensometer technology coupled with a high-resolution displacement instrument called a Differential Variable Reluctance Transducer (DVRT) to observe change in soil displacement, the need for specific geologic conditions is reduced. Although this technique is more limited by the properties of the formation than one measuring both solid stress and ground water pressure simultaneously as suggested by van der Kamp and

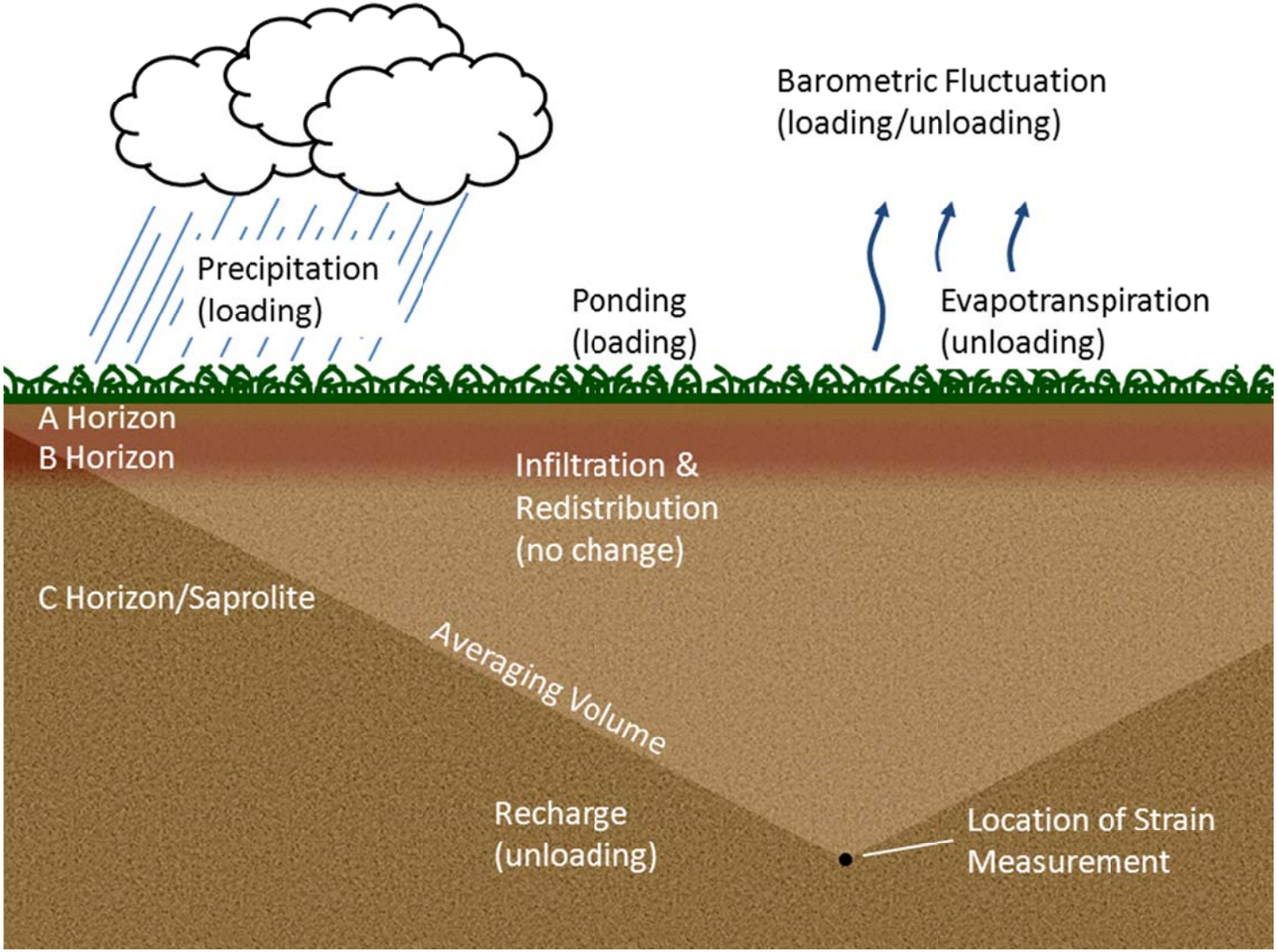

Figure 1. Conceptual model for using displacement measurements to observe hydrologic processes

Schmidt (1997), the DVRT is expected to be capable of detecting changes in soil moisture content of 1 mm or less at our field sites. Further, site-specific design modifications are expected to allow similar resolution at most sites underlain by unconsolidated soils.

Theoretical Analysis

The concept of measuring vertical displacement of the soil matrix to infer the load change takes advantage of the relationship between stress and strain in a solid. According to Hooke's Law, the stress in a solid is linearly related to the strain for small displacements (Hibbeler, 2005), and thus for a given load there is a corresponding strain or displacement. The displacement can be correlated to an applied, known load and then used to estimate unknown loads.

Two key behaviors of the system are the averaged response at a point in the subsurface to a distributed load at the surface and the scaling of the sampled region with the depth of the monitoring point. Because the effect of the load diminishes as the load departs from the monitoring point, the measurement represents a weighted average centered about the monitoring point, and there is a finite loading area for which the soil response will be measurable. The radius of the loading area is proportional to the depth of the monitoring point such that the scale of the measurement can be controlled by the depth of the instrument. These behaviors are described by the Boussinesq solution for vertical deformation in a half space induced by a point load at the system boundary (Davis and Selvadurai, 1996). This displacement is given by

$$\delta = \frac{P}{4\pi G}\left[\frac{2(1-\nu)}{R} + \frac{z^2}{R^3}\right] \tag{2}$$

where P is the magnitude of the vertical component of the point load, G is the shear modulus of the half space, ν is the Poisson's ratio of the half space, z is the vertical distance from the half space boundary to the point of interest, and R is the resultant between the point of interest and the point at which the load is acting. The corresponding stress is given by

$$\sigma = \frac{P}{2\pi}\left[\frac{3rz^2}{R^5}\right] \tag{3}$$

Where r is the distance in the horizontal direction from the point load to the point of interest. The point load P may be replaced by the product of a distributed load W [N m^{-2}] and the horizontal area over which the load acts A [m^2]:

$$P = WA \tag{4}$$

If this distributed load is infinite, Equation 3 becomes

$$d\sigma = \frac{W}{2\pi}\left[\frac{3rz^2}{R^5}\right]dA \tag{5}$$

which, when integrated through horizontal space yields the condition for static equilibrium given by

$$\sigma = W \tag{6}$$

The one-dimensional Hooke's Law states that stress is linearly proportional to the strain

$$\sigma = E\varepsilon \tag{7}$$

and

$$\varepsilon = \frac{\delta_s}{L} \tag{8}$$

where E is Young's Modulus, ε is the strain, δ_s is the observed displacement of the soil, and L is the length of the interval over which the displacement is measured. Substituting Equation 6 into the 1D form of Hooke's Law yields

$$W = E\frac{\delta_s}{L} \tag{9}$$

where E is the modulus of elasticity and L is the length of the interval being measured. Equation 9 may be used to estimate either W or E.

Poroelastic effects are expected to influence the displacement. Atmospheric pressure will load the ground surface and cause displacements at depth, but as the pore pressure equilibrates with atmospheric pressure, the stress on the solids will be relieved and the displacement will rebound. Likewise, when the solids are loaded, the pore pressure will increase and bear some of the load. The solid displacement will then gradually increase as the pore pressure equilibrates (Detournay and Cheng, 1993) creating a delay between the initial and equilibrated displacement signal that depends on the diffusivity of the soil. Another transient effect that scales with the diffusivity will occur when a change in atmospheric pressure propagates from the ground surface downward (Wang and Hsu, 2009).

Typical diurnal barometric fluctuation is on the order of 500 Pa (5 mm water equivalent loading), which in saprolite which has a modulus ranging from 10^7 to 10^8 Pa (Albers, 2010; Ng and Leung, 2007; Das, 2006) could cause soil displacements on the order of microns, similar to the effect of a light rainfall or ET. This suggests the need for

a method to remove the barometric effect. This may be done either by measuring the effective pressure loading caused by differential pressure between the atmosphere and the pore space directly or by applying the diffusion equation to estimate bulk loading of a porous medium. Each installation is equipped with a differential pressure transducer, and a collaborator has developed an analytical solution for soil strain response as a function of barometric pressure. Where possible, both techniques will be applied to the data and compared.

CHAPTER 2: METHODS

The major tasks of this research were to design and build a prototype; to test the prototype, revise the design, and begin monitoring a field site; and to evaluate the observed field data. This required a robust design for a device and a repeatable method for installation, data acquisition, data processing, and data interpretation. Lab-scale experiments were conducted for the purpose of preliminary evaluation prior to field installation. Field experiments were used to evaluate the performance of the Sand-X.

2.1 Instrument Design

The goal of the preliminary design process was to assemble a list of functions and criteria describing the end product and to develop an instrument that could be used to measure the displacement of soil at a resolution representative of loading due to soil moisture change. This section describes the current design and highlights the key aspects of and considerations for the design.

The functions are the tasks the instrument must perform in order to make the measurements required, and the criteria and constraints of the design are the standards to which the design must perform these tasks for it to be considered successful. Constraints must be met during the early stages of design and research to consider this approach successful. Criteria should be met during later revisions of the design for the approach to be practical, but for the purposes of this research, it was acceptable for the results to approach these standards without meeting them.

Functions

The instrument must…

1. Anchor. The instrument must anchor to the soil at two locations. This component of the instrument will establish a measurement interval and ensure that changes in this interval are controlled by the soil alone.
2. Contact the Transducer Probe. The instrument must provide a means of contact with the transducer probe or equivalent. The surface of this component must be suitable for making small displacement measurements, for example in terms of roughness, squareness, reflectiveness, etc.
3. Retain the Transducer. The instrument must provide a means of mounting the transducer reliably, repeatably, and securely to the anchoring system.
4. Span the Anchor Separation. The instrument must provide a means of spanning the gap between the sections which are anchored to the soil. This will enable the probe to connect to the anchoring system at both soil-anchor connections, regardless of the separation between these locations.
5. Decouple the Non-anchoring Sections. The instrument must include a means of decoupling the body of the instrument from the soil. Friction between the body of the instrument and the soil could hinder the movement of the anchoring system.

Constraints

1. Scalability. The device must allow scalability of the sampling region in a predictable way, e.g. linearly such that the linear coefficient can be determined. Because the emphasis of this research is on estimating soil moisture changes at a scale not traditionally possible with long-term measurements, it is paramount that

the instrument be capable of taking advantage of the soil stress distribution at depth.

2. Resolution. The instrument must be capable of resolving 10^{-8} m of displacement. The cutoff will be determined by the RMS error about a linear trend line through 5 minutes of data obtained at 1 Hz. This will allow the device to resolve 1Pa of load change—comparable to the equivalent resolution of a tipping bucket rain gauge—applied to soil with a Young's Modulus of 10^{8} Pa, assuming the device is 1 m long. The resolution may be further improved by lengthening the device.
3. Drift. The device must be capable of making measurements for months or years with drift that is no greater than 25% of the long term signal at this time scale. Specifically, average precipitation measured in Anderson County, South Carolina for the last fifty years was 1262.1 mm $year^{-1}$ (Purvis, 2010) and average evapotranspiration estimated by scaling pan evaporation by 70% was 918.7 mm $year^{-1}$ (Purvis, 2010) for a net increase of 343.4 mm of water $year^{-1}$. A drift of 25% would produce an error of 85.85 mm $year^{-1}$ for signal at this magnitude—over 100 times the anticipated resolution of the instrument.
4. Anchoring. The device must connect to the soil at two locations so that the force required to free the anchors from the borehole is no less than the greater of 10 times the weight of the instrument and the force required to pass the instrument through 20 times the full scale of the displacement transducer. Once this condition has been met, the instrument must demonstrate that it responds repeatably to precipitation.

Criteria

1. Decoupling. The device should incorporate a component to reduce the friction between the body of the instrument and the soil. Friction between the device and the soil may prevent representative measurements of the behavior of the soil.
2. Installation. The instrument should be capable of being installed in a borehole created with a Geoprobe, or similar small drilling rig, to depths of at least 5 m in saprolite. Installation at less than about 30 m should be simple and inexpensive and should require minimal time commitment.
3. Component Interchangeability. The components should be modular such that only sections of the device require redesign for customized applications. By designing the device for customizability, modifications will be simpler to design and implement. For example, the connecting component which spans the gap separating the anchors should be extendable to allow the site and application to define the spacing between the anchors.
4. Size. The device should begin as sections no longer than 2 m and no larger in diameter than 15 cm. This will benefit the end user because the effort required to install the device depends on the size of the device. A relatively small instrument is easier to transport and install.
5. Density. The density of the device should match the density of the soil as closely as is practical. Following installation of the instrument, the borehole will settle, but this process may be prolonged if the weight of the device causes the soil to creep.

6. Temperature. The coefficient of thermal expansion of the device should match that of the soil as nearly as is practical. Temperature variation will cause the Sand-X core to expand or contract, introducing error in the measurement that scales with the length. By selecting a material that behaves in a similar manner to the soil around the instrument, these effects can be minimized.

The Sand Extensometer

The instrument that is being developed for this research is called a Sand Extensometer, or *Sand-X*. The Sand-X is designed to measure displacement of unconsolidated material. It is composed of two anchors separated by a 1.5-m-long fiberglass rod, or "core", which is fixed to one anchor and centered along the axis of the instrument as shown in Figure 2. A centralizing housing containing the DVRT is

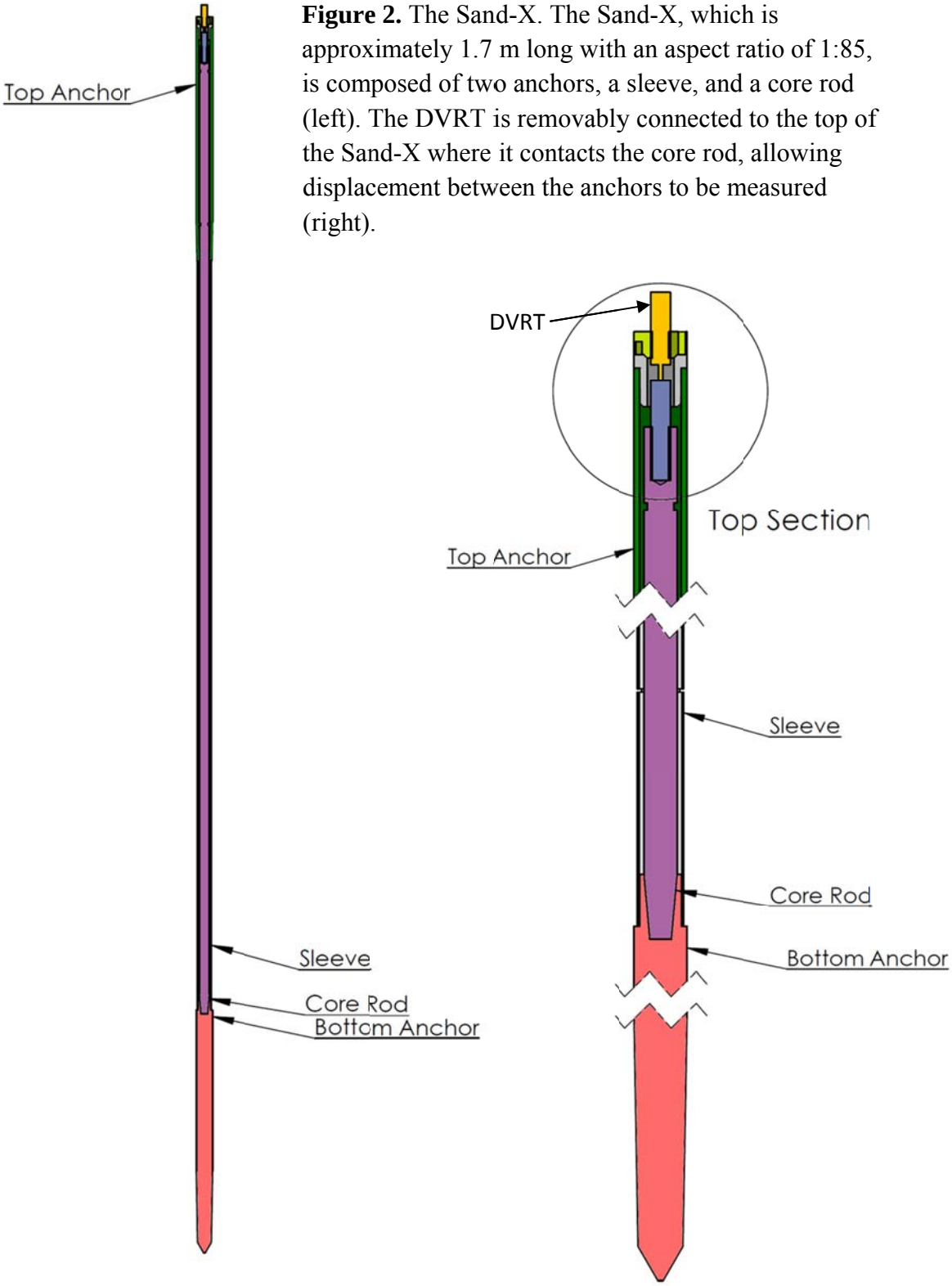

Figure 2. The Sand-X. The Sand-X, which is approximately 1.7 m long with an aspect ratio of 1:85, is composed of two anchors, a sleeve, and a core rod (left). The DVRT is removably connected to the top of the Sand-X where it contacts the core rod, allowing displacement between the anchors to be measured (right).

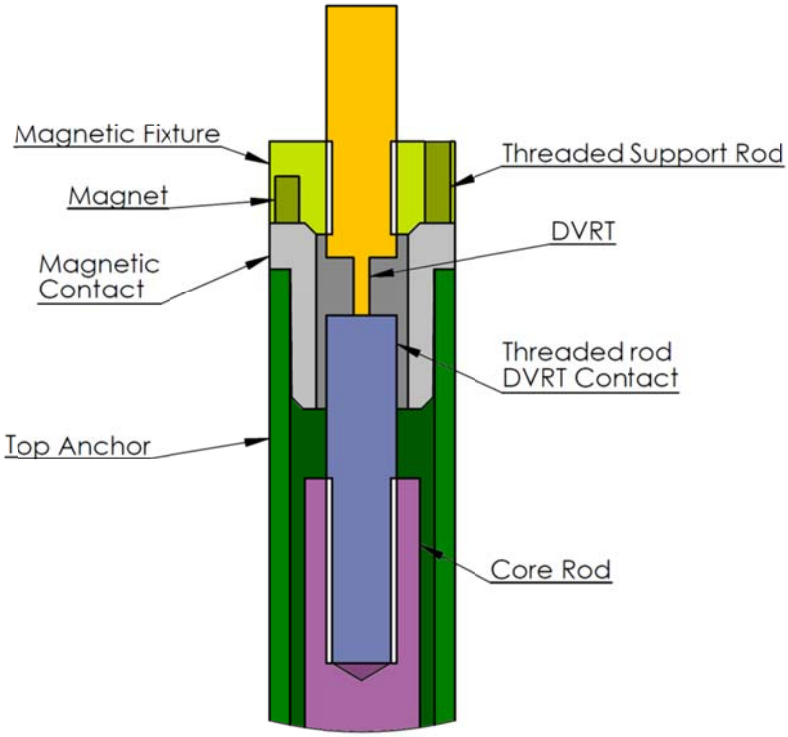

Figure 3. Top section of the Sand-X. The DVRT is magnetically connected to the top anchor where it measures displacement between the anchors.

magnetically fixed to the upper anchor such that the transducer probe contacts a stainless steel contact surface at the end of the fiberglass rod. This steel contact surface is the machined end of a 3/8”-16 bolt epoxied into the fiberglass rod; this bolt is used to lower the Sand-X to the bottom of the casing. The device is deployed axially in a 2-cm diameter open borehole, and the 2.5-cm diameter anchors, which fit snugly into the borehole, grip the soil matrix by friction. This is accomplished by employing a long, shallow taper on the leading edge of the anchors which gently expands the hole as the anchors are pushed into the ground. The measured displacement can be used to calculate the vertical strain in the matrix, and by calibrating the Sand-X measurements under known loads, the strain

can be used to estimate changes in distributed surface loads and the corresponding changes in effective stress.

The approach used to anchor the Sand-X to the soil was to make the anchor slightly larger than the hole to create a force-fit connection between the soil and the anchor. By incorporating a gradual taper over the bottom section of the anchor, a tighter fit between the anchor and the soil can be achieved without the risk of damaging the Sand-X during installation.

The force required to dislodge an anchor that uses this force-fit design can be estimated by calculating the normal stress of the soil, estimating the resulting shear stress between the anchor and the soil, and multiplying the shear stress by the area of contact between the anchor and the soil. The hole diameter into which the anchors were driven was approximately less than 2 cm which gives 20% strain for a 2.5 cm anchor. For a more conservative strain of 10% and assuming roughly that the soil behaves elastically, the soil stress resulting from the emplacement of the anchor may be calculated by Equation 7. For saprolite ($E = 10^7$ Pa), this gives $\sigma=10^6$ Pa. The maximum shear stress τ that would prevent the anchor from being dislodged is

$$\tau = f\sigma \tag{10}$$

where f is the friction coefficient. If the friction coefficient is assumed to be 0.1 (a conservative estimate), the shear stress to dislodge the anchor is 10^5 Pa. By the definition of shear stress

$$\tau = \frac{F}{A} \tag{11}$$

where F is the shear force and A is the area of contact between the soil and the anchor. For an anchor length of 30 cm, the area is approximately 240 cm^2, and by solving Equation 11, the force required to dislodge the anchor is approximately 2.4 x 10^3 N.

The core rod, which closes the gap between the anchors, provides a means of measuring the displacement between the anchors. In particular, the core rod provides flexibility to the spacing between the anchors by providing a simple means of lengthening the instrument with extensions. The material used for the core rod is structural fiberglass which seems to mimic the soil density and thermal expansion properties well enough for a preliminary trial. The fiberglass had a nominal density of about 1600 to 1950 kg m^{-3} (McMaster-Carr, 2011). The density of saprolite in the Carolina piedmont is around 1500 kg m^{-3} (Kirtland *et al*., 2001; Schoeneberger and Amoozegar, 1990). For the purposes of preliminary experimentation, this was considered sufficient similarity. The fiberglass has a thermal coefficient of expansion of 8 μm $m^{-1}°C^{-1}$, which, for example, is roughly an order of magnitude greater than that of silica and on the same order of magnitude as granite, quartz, and iron. Though it is necessary to characterize the soil on site more carefully, this is sufficient for preliminary experimentation in the temperature-stable subsurface.

The sleeve helps to isolate the core rod from the soil surrounding the instrument to prevent interference to the measurement. The sleeve will be a thin-walled aluminum tube with slots cut on alternating sides about three-quarters of the way through the tube and perpendicular to its axis. They will reduce the stiffness of the aluminum so that the axial stiffness of the tube is less than 1% of the stiffness of the soil. Though the slots will

allow some soil to fall off into the sleeve, the soil formation will be held away from the core rod.

2.2 Installation Design

The process of installing a Sand-X occurred in three phases: drilling and completing the borehole, coring the secondary borehole and installing the Sand-X in this boring, and installing and routing the electronic equipment. The purpose of the borehole was to provide access to the soil at depth where the Sand-X is installed. Following installation, the hole provided access to the device and accompanying electronics while limiting exposure of the electronics and Sand-X to moisture and thermal variation.

Borehole Design

The boring for pilot field installations was a two-inch casing installed in a four-inch borehole. The one hole extended down to 1.5 m below ground surface and two other holes were drilled to a depth of about 6 m. The bottom of each of the holes was cleared of debris using a hand auger. The casing was schedule 40 PVC pipe that were prepared with centralizers made with three heavy-duty zip ties, each parallel to the casing, at intervals of 120° around the casing from each other, and clamped to the casing with hose clamps such that the zip ties bubbled out to just touch the walls of the hole. These centralizers were placed at 2.5 m intervals with the first at the bottom of the casing and the last fixed to the casing near the ground surface. A PVC funnel, which reduced the inner diameter of the casing from 5 cm to 2.8 cm, was cemented into the bottom of the casing to guide the Sand-X and tooling to the same centralized location at the bottom of the casing. A 10-cm-

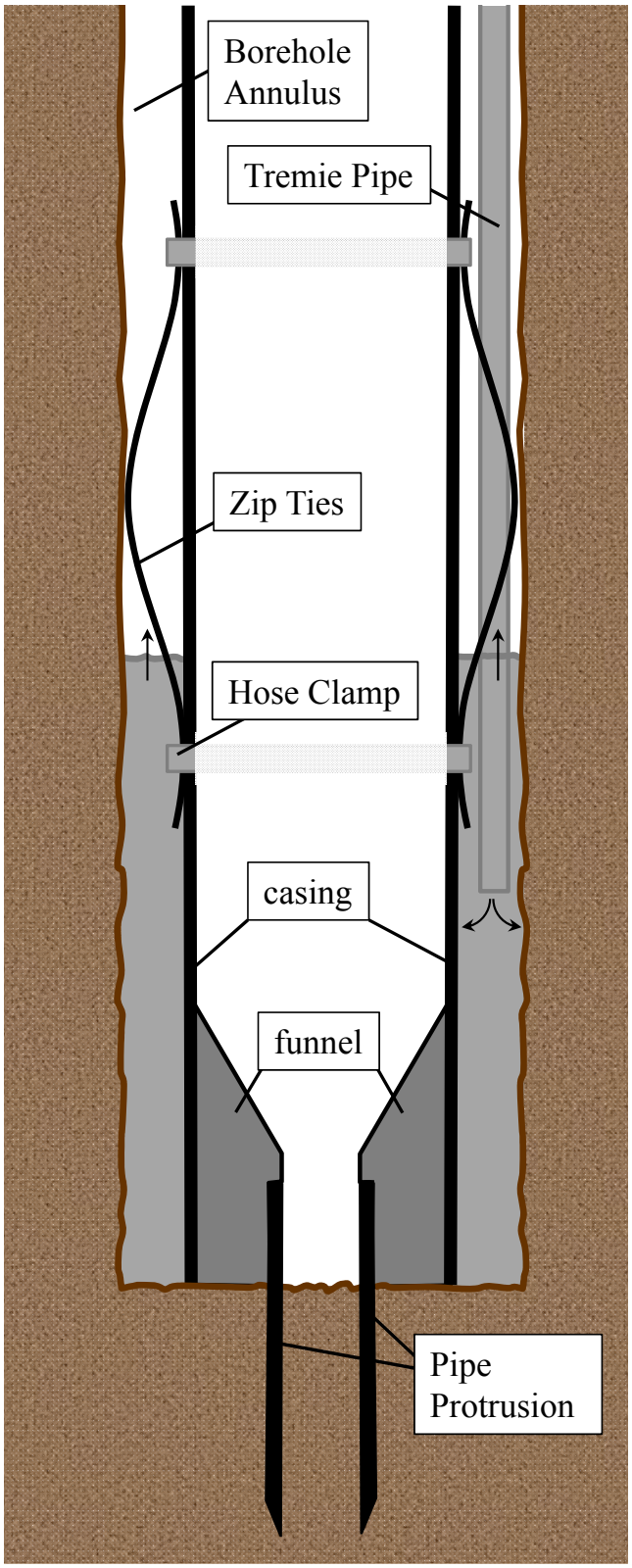

Figure 4. Borehole design. The casing is centralized in the borehole while the borehole annulus is filled with cement; a pipe protrusion prevents the cement from flowing into the casing.

long section of PVC pipe with 2.8 cm inner diameter was fixed to the inside of the funnel such that it extends below the bottom of the funnel by 5 cm. This extension protrudes into the soil below the 4-inch boring as shown in Figure 4. The casing was fixed in the borehole with neat cement which fills the boring annulus.

Electrical System Design

The electrical system is composed of borehole electronics and weather electronics. Each system is composed of signal conditioning and data logging components, power supply and distribution components, and sensors. The strategy was to include, in addition to the displacement equipment,

as many peripheral sensors as was practical, each sampling at the minimum rate, between 1 and 5 minute spacing, and resolution required to obtain useful information for comparison to the displacement measurements. Because the study requires continuous data collection for months, sampling at a higher rate or resolution than necessary would have the effect of making the datasets more cumbersome. Because of the difference in sampling rates and the quantity of sensors, three data loggers were used. One data logger collected high-resolution pressure, temperature, and displacement data at a rate of 1 sample per minute while the other two collected lower resolution weather data at a rate of once per 5 minutes.

The DVRT provided the foundational measurements of displacement from the Sand-X. Because the soil was expected to have a stiffness of greater than 10^6 Pa, the displacement measurements were collected with the goal of obtaining the highest resolution possible. Likewise, a sampling rate of 1 Hz was maintained for the first four months of trial. Subsequently, the sampling rate was lowered to 1 sample per minute. The DVRT outputs a frequency signal which was demodulated to a voltage and then converted to digital with a 24-bit Symmetric Research analog to digital converter, model SER1CH-UA-1in.

The high-resolution electronic sensors—barometric and differential pressure and borehole temperature—were grouped with the Sand-X electronics. The reasoning for this was that these were the factors that were expected to produce the greatest spurious signal in the displacement measurements. Borehole temperature was required at a high resolution to provide a means of comparing fluctuation in the displacement signal to

fluctuations in borehole temperature. The DVRT fixture, which was made of aluminum and was about 2.5 cm long, was expected to expand and contract at a rate of about 5 x 10^{-7} m $°C^{-1}$, indicating that even small changes less than 1°C would have a significant impact on the signal compared to the resolution of 10^{-8} m called for in the criteria. Likewise, typical diurnal barometric fluctuations of 500 Pa are two orders of magnitude greater than the desired resolution specified in the criteria. Consequently, differential and barometric pressure must be known to a great degree of accuracy as well.

The high-resolution electronics were collected by a Campbell Scientific CR800 data logger which was stored with other surface electronics in an enclosure a short distance from the borehole. The data logger was connected to a small laptop computer which was scheduled to collect data from the logger at an interval of 3 hours to provide data security. The data logger was powered by an unregulated 12V power supply which was stepped down to 9V by a high-quality voltage regulator to power the sensors. The 9V regulator also powered a small fan that kept the computer cool to prevent it from freezing.

Special considerations for wire and tubing routing were provided for the DVRT, differential pressure transducer, and temperature sensor which were emplaced in the casing. Signal and power for all of the sensors was transmitted through a primary communication line in the form of a CAT5 cable which was routed into the well with the electronics. The DVRT required demodulation and conversion to digital signal before being transmitted to the data logger to minimize noise in the signal. The demodulator and analog to digital converter were contained in an enclosure which was suspended by a

wire from the borehole cap within the casing. The temperature sensor which was suspended below this enclosure near the DVRT received power and transmitted data into the enclosure where the wires were connected to the CAT5 cable. The differential pressure transducer was suspended in the casing above the enclosure. It received power from and transmitted data to the CAT5 cable through a splice in the wires. Two tubes were connected to the differential pressure transducer—one passing out of the casing to access atmospheric pressure and the other remaining in the casing to access borehole pressure. The transducer measured the difference between the two.

The weather sensors are sampled at a rate of 1 sample per 5 minutes using an Em50 and an Em5 data logger. This was deemed sufficient to provide enough data to correlate measured weather data to displacement data. Because spurious signals were expected to be large compared to the effect of precipitation and evapotranspiration, these measurement parameters were considered appropriate for a preliminary evaluation of the response of the Sand-X to weather. Precipitation at a centralized, primary weather station and soil moisture spaced in a circle about 8 m from the base of the weather station were sampled for direct validation and correlation of the response of the soil to changes in the system. Wind speed and direction, solar radiation, relative humidity, and air temperature, all fixed to the centralized weather station, were measured to provide supplementary information as well. A soil heat flux sensor will be included in future datasets, providing all the necessary data to calculate evapotranspiration using the Penman-Monteith method for additional correlation to and validation of displacement signal.

2.3 Installation

Borehole and Casing Installation

The first hole was bored by hand using a four-inch auger, and subsequent holes were drilled using a Geoprobe drill rig and solid-stem augers. The casing sections were lowered into the hole one at a time, and a new section was connected with standard slip-fit couplings cemented to the pipe before lowering the casing further. Once the casing was at the bottom of the hole, the tooth was driven into the soil at the bottom of the hole, creating a region where the top of the Sand-X would be isolated from the soil and preventing cement from flowing up into the well during the completion process

With the casing in place, the annulus of the borehole was filled with cement. Ideally, the weight of the cement will create a compressive stress on the soil that is similar to the compressive stress created by the weight of the soil itself. Portland cement was used in a mixture of 43 kg cement to 14 L of water. To ensure that the cement filled the annulus completely and prevent the formation of air pockets, a tremie pipe was used to pump the cement to the bottom of the annulus to the top of the borehole.

Sand-X Installation

A hole was cored into the soil below the casing for the Sand-X. The hole was created using an AMS model 401.15 soil sampler which has a diameter of 22 mm, connected to a slide hammer with extensions. The soil sampler was guided to the center of the casing by the funnel at the bottom of the well, ensuring that the Sand-X boring was aligned with the axis of the casing.

A vacuum system was used to clean the funnel of soil that accumulated in the casing during coring of the secondary borehole. Soil between the DVRT housing and the contact surface on the top anchor and connection rod would interfere with the measurement and reduce the reliability of the connection between the DVRT and the Sand-X, so as much soil as possible was removed prior to installation. The vacuum system was composed of 1-inch PVC pipe, which extended from the ground surface to the bottom of the casing, with a customized vacuum head attached to the bottom and a vacuum connected by a hose to the top as shown in Figure 6. This system was allowed to rest in the bottom of the funnel while a mark was drawn on the 1-inch pipe at the top of the casing. The length from the bottom of the funnel to the top of the casing could then be measured at the surface to ensure the Sand-X was installed to the correct depth.

Figure 5. Customized vacuum head.

Figure 6. Removing soil from the funnel with a vacuum. The vacuum head and extension pipe are shown in place. In this position, soil was removed from the funnel and protrusion, and the depth from the top of the casing to the funnel was marked on the extension pipe.

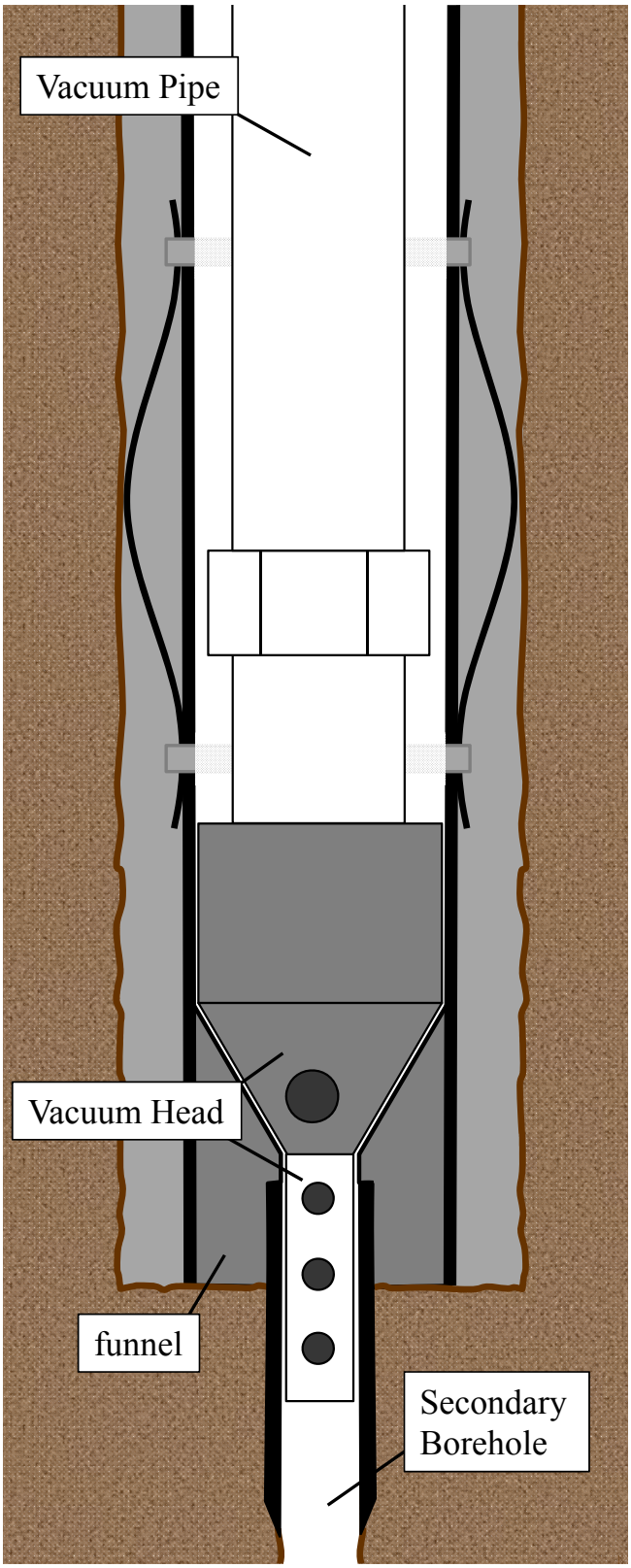

The Sand-X was installed using AMS extensions and a slide hammer. Before lowering the Sand-X into the borehole, it was laid out on the ground along with the extensions and slide hammer. The sections were each measured, and a mark was placed to indicate the depth at which the Sand-X was installed properly. An adapter that was machined for installing the Sand-X connected the 3/8" threaded rod on the Sand-X to the 5/8" AMS threads. The adapter was threaded onto the Sand-X by hand until it stopped so that it would be loose enough to unthread with the Sand-X installed. The other end of the adapter was connected

tightly to the extension rods using wrenches, and the adapter was secured to the extension further by wrapping the joint with duct tape to ensure that this connection would *not* come loose during the installation. The same approach was taken each time an extension was added as the Sand-X was lowered. With the Sand-X resting in the funnel at the bottom of the casing and the top of the lower borehole, a slide hammer was connected to the top extension. Using the slide hammer, the Sand-X was forcefully driven into the lower borehole until the depth marker was aligned with the casing, indicating that the Sand-X was installed to the correct depth.

Electronics Routing and Installation

With the mechanical components of the Sand-X in place, the casing above the Sand-X was available for deployment of data acquisition electronics and other sensors. The casing was sealed from the atmosphere with a pass-through connector fixed to a cap at the top of the casing. The data cables and differential pressure tubing were routed through this connector. If the pore pressure is allowed to equilibrate with atmospheric pressure, it may cause unusual system behavior that could obscure signal. The borehole electronics were suspended from the cap by a coated steel wire. The down-hole components are accessible from the surface by disconnecting the casing head, lifting it from the top of the casing, and pulling the electronics out by this wire.

2.4 Data Collection

Although the purpose of this research is to evaluate the feasibility and performance of this new technology, an accurate assessment will not be possible without

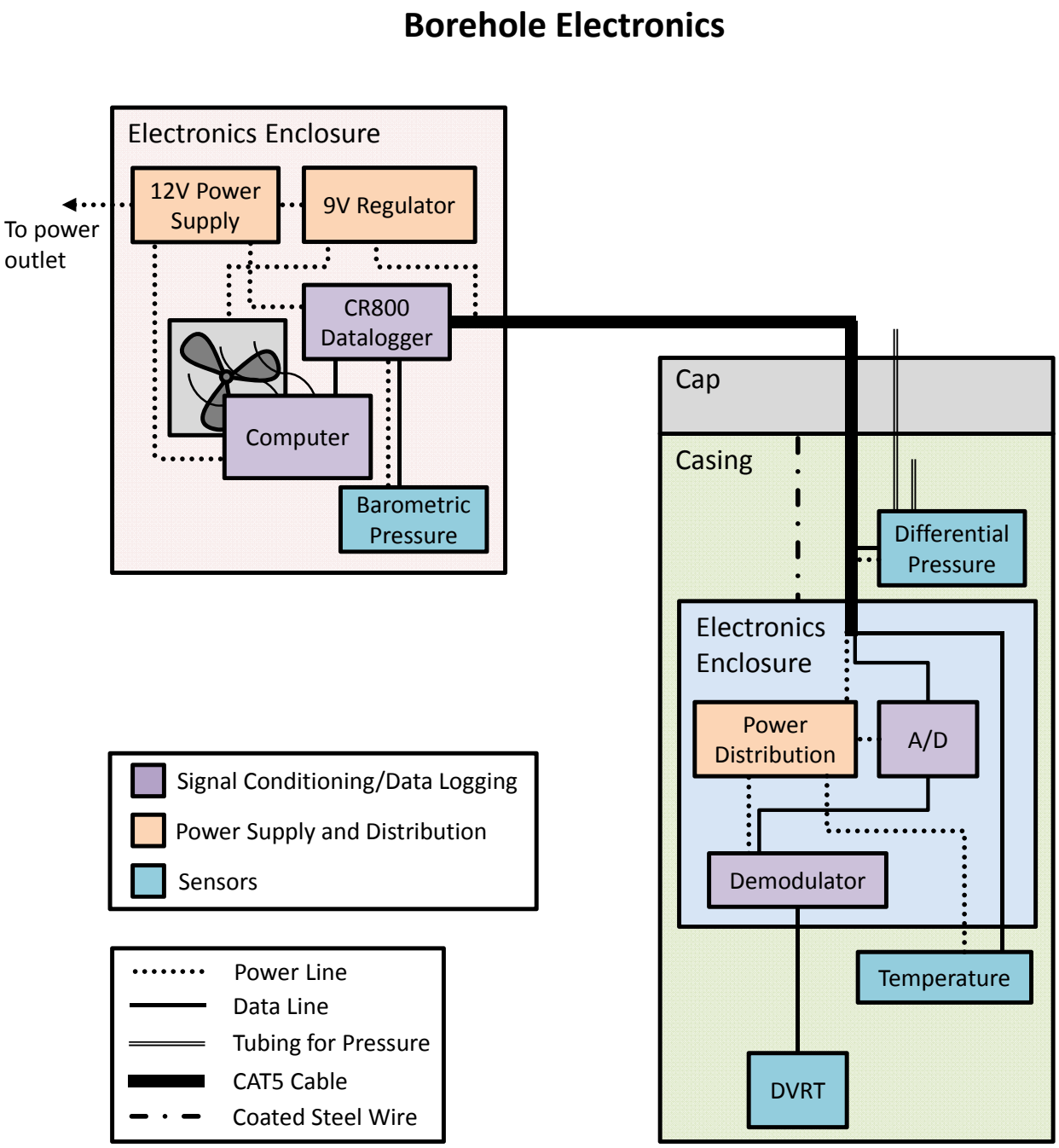

Figure 7. Borehole electronics schematic.

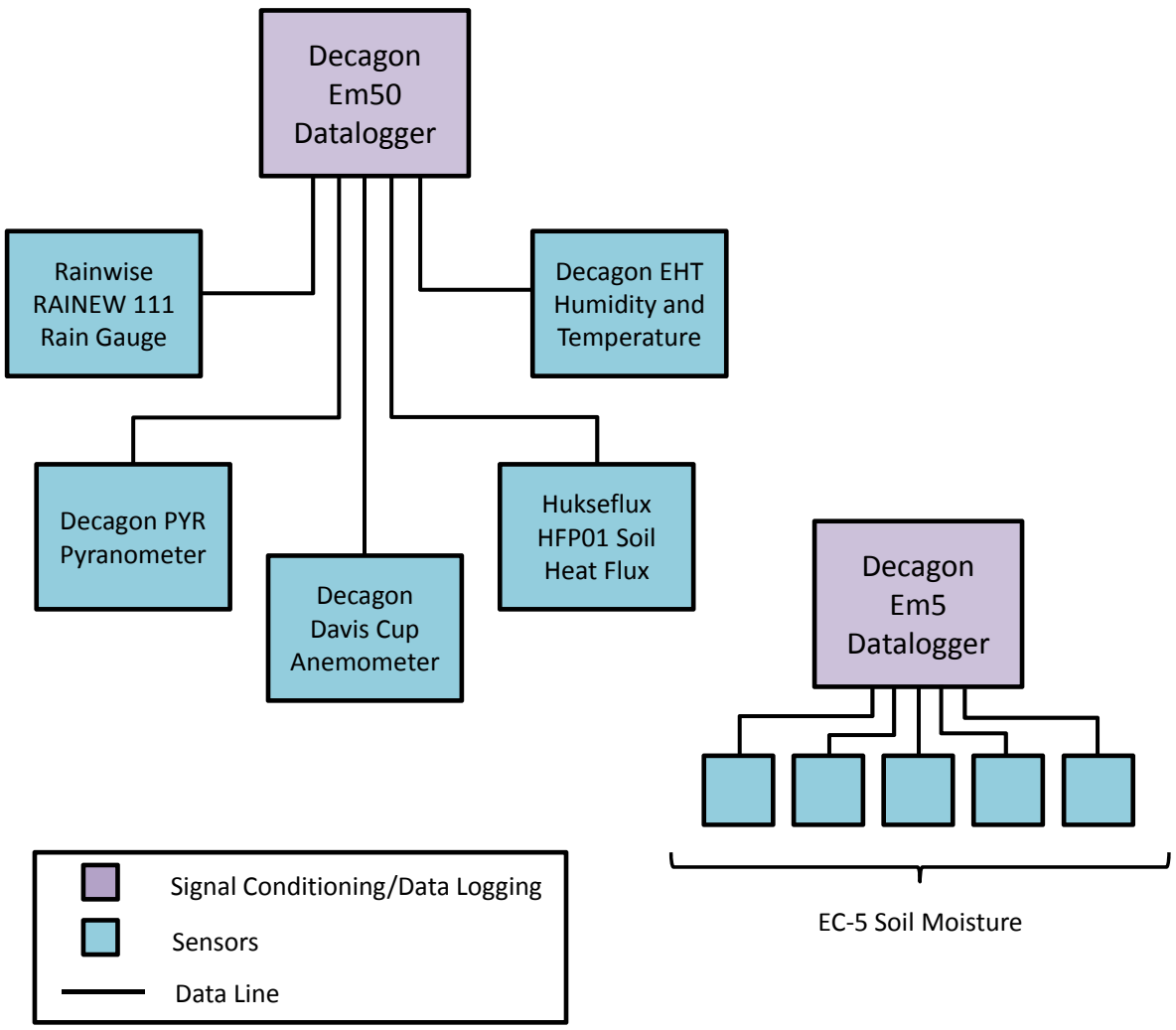

Figure 8. Weather electronics schematic.

a robust method for acquiring, processing, and storing the measurements from the device. Consequently, the methods used for this facet of the research must be chosen with care. While standard methods for acquiring data may be reliable, alternative data acquisition systems will also be considered for their customizability to the unique set of electronics

that will be used for this research. Data file storage, meta information, and processing standards will also be determined early and maintained for the duration of this research.

Displacement Electronics

The displacement measurements are performed with a *differential variable reluctance transducer*, or DVRT, with a measurement span of 0.5 mm. The DVRT has an accuracy of ±500 nm and a resolution of up to ±5 nm in thermally stable conditions. The output signal from the DVRT is frequency response which is converted to a voltage signal by a demodulator. To ensure signal stability while minimizing error of the signal, a 24-bit A/D board is used to convert the voltage signal to a digital signal that can be stored by a computer or data logger.

Concurrent Measurements

A set of environmental measurements are taken concurrently with the displacement measurements for validation, correlation, and removal of spurious signal. Weather is expected to have the most significant effect on the behavior of natural systems. Consequently, the data set is composed of on-site weather data in addition to displacement measurements. The measurements that are included in the data set are atmospheric temperature and pressure, precipitation, solar radiation, humidity, wind speed and direction, borehole temperature, and differential pressure between the pores surrounding the Sand-X and the atmosphere.

Data Logging

A Campbell CR800 data logger was chosen as the most appropriate data logging system for the displacement and borehole measurements. This logger stores data in a standardized format and is capable of measuring data from multiple installations simultaneously. In addition, it only requires about 1 mA of current, making it ideal for remote data sites where the power is supplied by a solar power system. The Campbell CR800 is capable of running user-customized programs that can control detailed aspects of the communication between the logger and peripheral devices. This makes access to the customized electronics used for making displacement measurements possible.

Because of the application for research involving multiple displacement measurements, wireless data transmission technology is being considered for future installations. This approach would allow data from many wells separated by thousands of meters to be collected by a single hub. This hub could then be connected to the internet, allowing it to store data in an online database.

Data Archiving

A standardized archiving format will be implemented to ensure that the data remains meaningful, both for future comparison of research and for sharing with the public knowledge base. The primary objectives of the format are to provide an unprocessed, complete data set to the public and to create a file structure that is efficient and simple to access. Redundant copies of the archived files will be stored on a local hard drive, a shared hard drive, and an internet drive to reduce the possibility of data loss.

Raw data files are converted to MATLAB variable files containing processed data. These files are stored together to provide the user with flexibility for accessing the data. The raw data allows the user access to the original measurements, and the MATLAB files provide the user with the ability to access the processed data efficiently. Along with the measured data, the MATLAB files include a metadata variable that describes the field site and conditions. This metadata variable includes the following information:

- Site name
- Identification numbers for each Sand-X at the site
- GPS coordinates to each Sand-X well at the site
- Site description
- DVRT identification numbers
- Beginning and ending timestamp for the dataset and units
- Sample rate of well instruments and units
- Calibration constants for the DVRTs
- Calibration constant for the analog to digital converter
- A list of the weather data included in the data set, the sample rate for each measurement, and units for the sample rate
- A list of indices to segments of data that were modified (removal of erroneous data points, etc.)

The purpose of this information is to make the data measurements as clear as possible for interpretation by the user.

2.5 Laboratory Experiments

Experiments at the lab scale were designed to give a clear picture of how the components of the instrument behaved under controlled conditions. This picture allowed us to better interpret field-scale data—signal that is largely uncontrolled. These experiments also divided the developmental stage of the research into small components that enabled a quick turnaround when troubleshooting was necessary. These experiments began with a study of the long-term response of the DVRT under thermally stable conditions which allowed us to estimate of the electronic drift that could be expected during field-scale operation. The second experiment added the Sand-X frame and was designed to examine the behavior of the Sand-X when load changes occurred. The third laboratory experiment examined the response of the Sand-X installed in soil to load changes at the soil surface boundary, giving us an idea of whether or not the device was ready for field deployment.

Sensor Noise

The DVRT was evaluated for noise by setting the probe half way through the full scale of the instrument, placing it in a thermally insulated container, and allowing it to sample at 1 Hz for days. A five minute segment of data after the initial equilibration period was selected, and a linear trend of 0.002 μm min^{-1} was removed from the data subset. The root mean squared error of this five-minute dataset was 0.0015 μm.

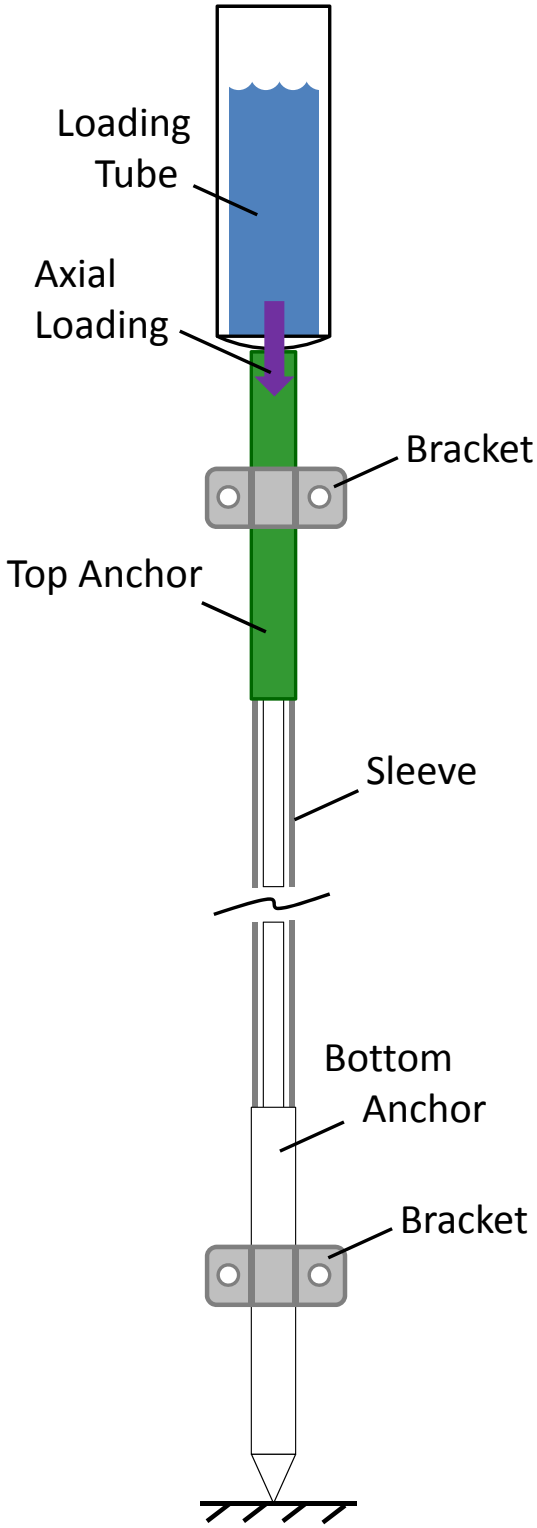

Figure 9. Sand-X compliance experiment apparatus. The Sand-X is oriented vertically by two brackets while an axial load is applied to the top anchor by a tube filled with water.

Instrument Compliance

The Sand-X must respond to soil displacement, but excessive resistance may cause the anchors to slip and obscure the signal. By design, the Sand-X acts like a spring which means that displacement will create a force that must be counteracted by the connection between the anchors and the soil. The compliance of the Sand-X prescribes a minimum stiffness of the soil-anchor connection to ensure that the anchors do not slip. The response of the instrument to displacement was measured by fixing one anchor, applying an axial load to the second anchor, and measuring the corresponding displacement.

This measurement was taken by aligning the axis of the Sand-X vertically

against a frame and by supporting it with two brackets that exert minimal axial force on the Sand-X as seen in Figure 9. The bottom anchor was sufficiently fixed in place by allowing it to rest on a cement floor. A PVC pipe which was capped on the bottom was placed on top of the upper anchor and also held vertically so that the weight of the pipe and its contents would be applied directly to the top anchor. The load acting on the anchor was changed by injecting increments of 10 mL of water to the PVC pipe while recording displacement until the Sand-X was compressed the full scale of 500 μm. The displacement measurements were offset so that the first data point (before loading) was zero. The compliance of the instrument, which was expected to behave like a linear spring, was estimated as the stiffest observed response.

The maximum stiffness of the Sand-X was -4 $\mu m\ N^{-1}$. For an average evapotranspiration rate of 6 mm da^{-1} (≈60 Pa) which is high for Clemson, South Carolina (Purvis, 2010), the displacement of a 1-m interval in a soil with modulus 10^7 Pa would be on the order of 6 $\mu m\ da^{-1}$ which translates to 1.5 N da^{-1}. This is approximately 1000 times smaller than the conservative estimate of the anchor dislodging force of 2.4×10^3 N.

Lab-Scale Response

The first Sand-X design was tested in a controlled laboratory-scale experiment designed to verify correct operation of the device. This was done by installing the Sand-X in compacted sand, loading the surface of the sand using a pressurized bladder, measuring the pressure in the bladder and the displacement of the Sand-X, and comparing the output of the two signals. If the displacement signal indicates soil compression that is synchronous with an increase in surface load and soil expansion that is synchronous with

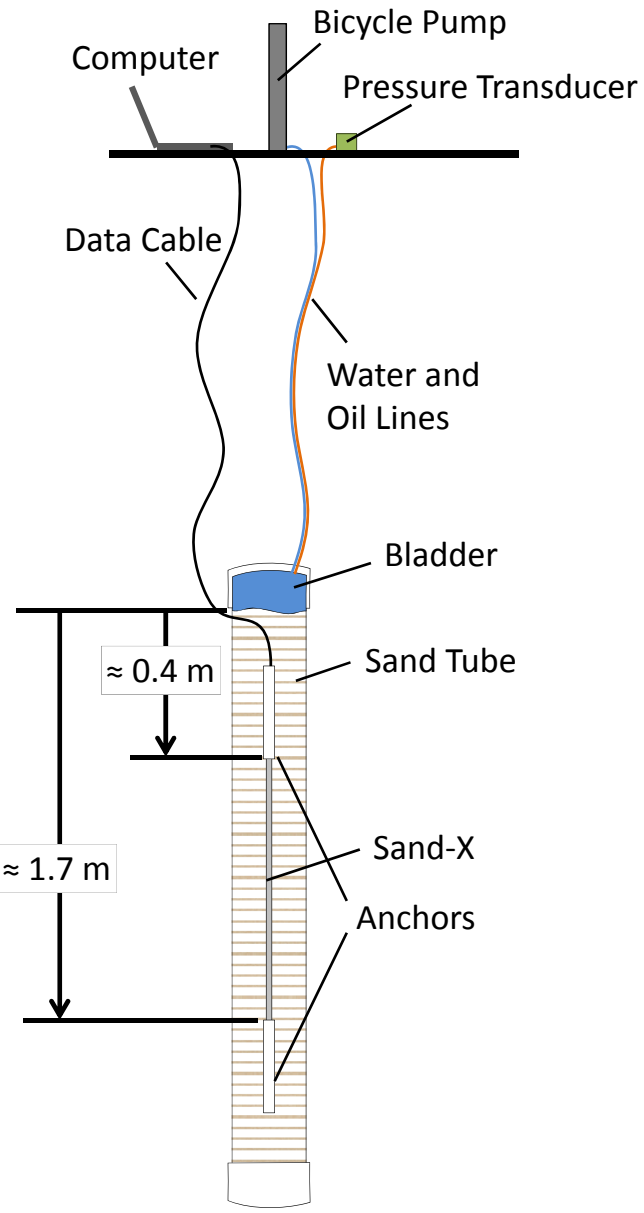

Figure 10. Sand tube experiment apparatus. The Sand-X was installed in a tube of sand which was loaded by a bladder of water pressurized using a bicycle pump; bladder pressure and displacement were measured during this experiment.

a decrease in surface load, the qualitative behavior of the device is consistent with the theoretical model of the behavior of the system.

The apparatus used in this experiment was an eight-foot long, 6- inch PVC pipe that was capped on the bottom and oriented vertically inside a wooden frame that supported the pipe. The Sand-X was placed in the center of the pipe buried with sand. The center three feet of the pipe were slotted, allowing the pipe to extend or compress freely in order to replicate a roller boundary, reducing the boundary effects on the mechanical behavior of the apparatus. A pneumatic vibrator was mounted to the column and run for a minimum of five minutes at no fewer than three positions along the length of the pipe to compact the sand. A plastic bladder

filled with water and connected to a bicycle pump and pressure transducer was placed inside the top of the pipe on top of the sand, and the top was fixed shut by the wooden frame. The bladder pressure was increased in increments of about 20 to 40 kPa using the bicycle pump while the pressure of the bladder and the displacement of the Sand-X were measured simultaneously.

2.6 Field Experiments

Field experiments at three sites were used to evaluate the performance of the Sand-X in natural settings. The focus of field experiments was on observing changes in distributed loading resulting from changes in soil moisture. Experiments involving point loads were performed for qualitative validation and to develop an approximate estimate of the elastic response of the system.

Field Sites

A field-scale pilot installation was completed at the Clemson Botanical Gardens Well Field, located adjacent to the Bob Campbell Geology Museum parking lot (34.667961, -82.827120). This site includes an equipment trailer and an enclosure that can both house computers and other electronic equipment. This site is downslope from a parking lot from which it receives surface runoff. The site is underlain by a layer of Cecil sandy loam which begins below the topsoil at 0.05 m and extends to about 3 m (USDA Web Soil Survey, 2012, 2012) before transitioning into the underlying formation. Underlying this layer is a layer of saprolite weathered from biotite gneiss that is about 22 m thick. The saprolite is underlain by the biotite gneiss parent bedrock which is fractured and hydraulically connected to the surface aquifer. The water table fluctuates around 6 m

below ground surface. The Sand-X at this site, labeled Sand-X 1, was installed in the Cecil sandy loam that overlays the saprolite. The top of the instrument is 1.5 m below ground surface, and the bottom anchor ends at 3.3 m from the ground surface in the transition from sandy loam to saprolite. The Sand-X borehole is positioned about 4 m south of the parking lot in a grassy clearing that is kept trimmed. A dogwood tree stands about 3 m to the NE of the installation, and a deciduous forest borders the clearing about 25 m to the south of the installation. A footpath which receives traffic daily runs along the edge of the forest.

The primary calibration, monitoring, and evaluation of the Sand-X was performed at the Simpson Station Bull Test Farm in Pendleton, SC (34.670018, -82.729311). The site is an open field with a forest about 75 m to the north. A large tractor shed about 25 m to the east of the installations provides access to power and houses the data acquisition electronics. The site is underlain by the Cataula sandy loam soil series, which extends 2 m below ground surface (USDA Web Soil Survey, 2012). This is underlain by a layer of saprolite weathered from biotite gneiss.

The site is covered by uncut grass and is dotted with deciduous saplings and evergreen shrubs ranging from 1 to 3 m in height. It is part of a 7.5 ha field from which it is separated by an electric fence. The field surrounding the site is kept short by cattle which are prevented from entering the site by the electric fence. The cattle are rotated periodically from one field to another such that their presence near the field site is infrequent and unpredictable. Farm vehicles occasionally drive past the electric fence as

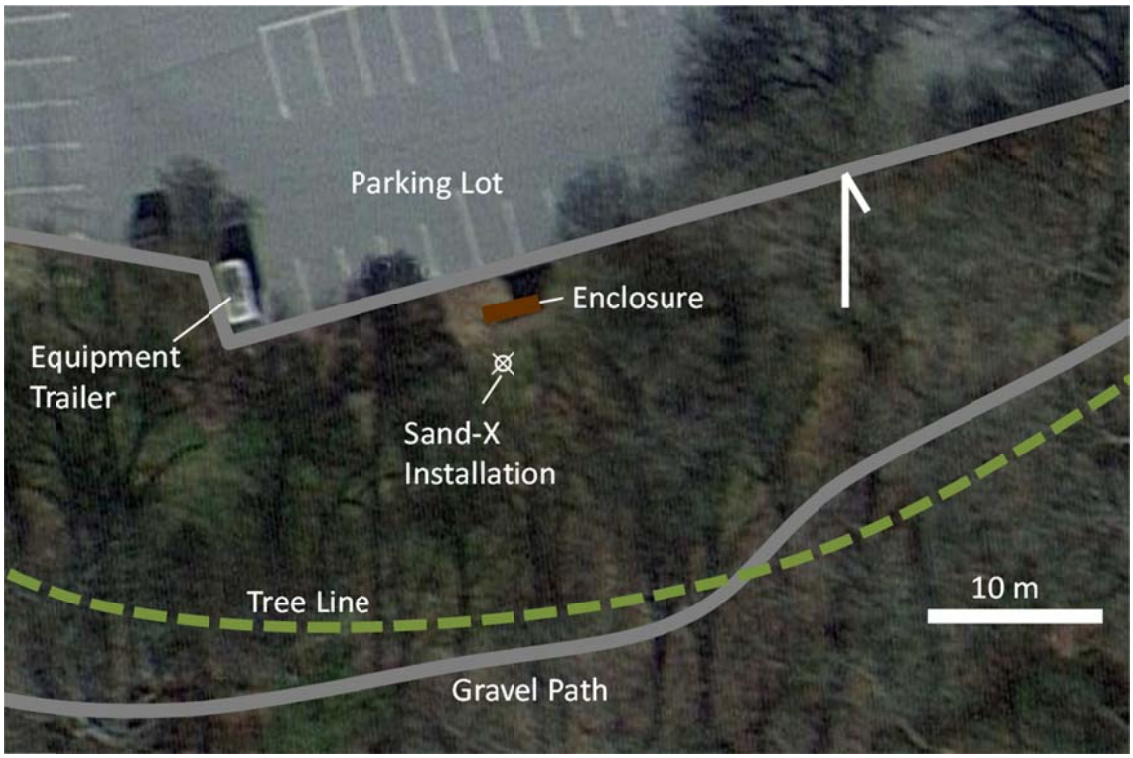

Figure 11. Maps of the Sand-X field sites. Map of the Clemson Botanical Gardens field site (above); map of the Simpson Station field site (below).

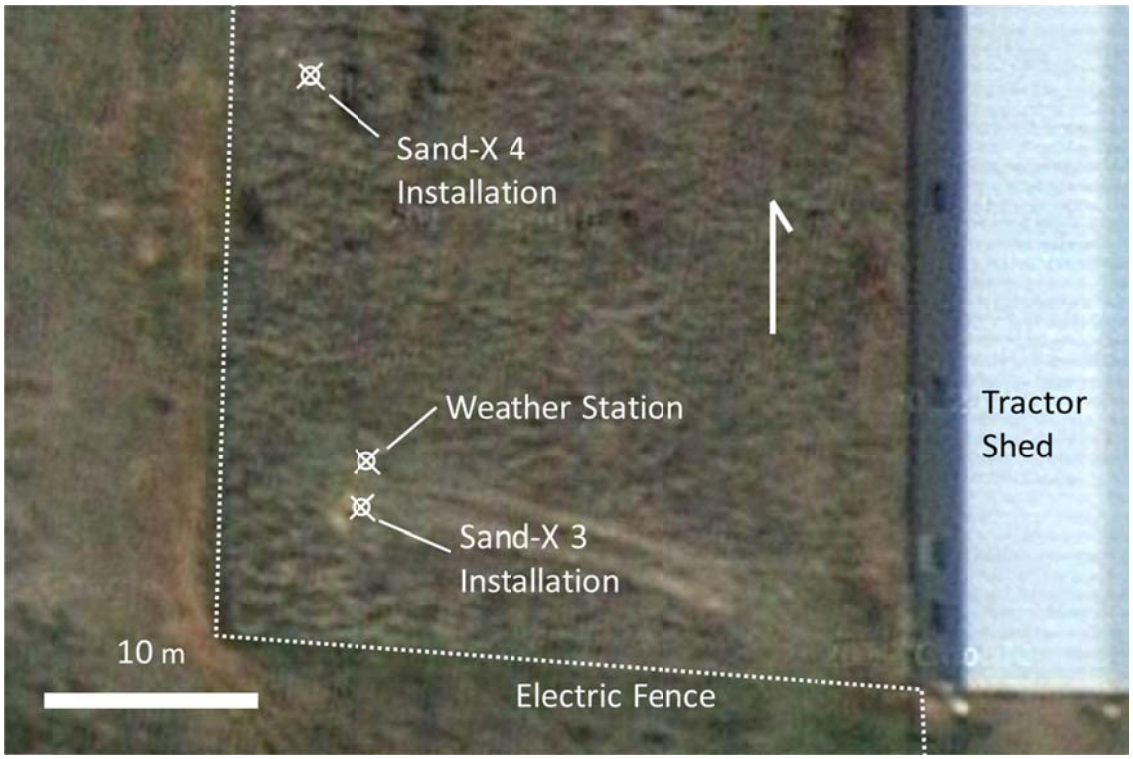

well. The first Sand-X installation at this site, designated Sand-X 3, was installed at a depth extending from 6 m to 7.8 m below the ground surface. This installation, located at 34.670067,-82.729662, is about 6 m from the electric fence. After about three months of nearly continuous operation, a second device designated Sand-X 4 was completed at a depth extending from 6 to 7.8 m below the ground surface about 22 m north of the first installation (34.670266,-82.729661). This instrument is approximately 2 m from the electric fence.

Point Load Calibration

For each installation, a preliminary, qualitative verification was performed to determine whether the instrument was sensitive to change in surface load. A 2001 Kia Optima with a weight of about 14,500 N was used as the point load representation. With the vehicle parked greater than 75 m from the casing access, a preliminary average displacement measurement was observed as displacement measurements were recorded at 1 Hz. Next, the vehicle was driven over the well and parked for about 30 s, and a second average measurement was observed as the average displacement over this period. Finally, the vehicle was removed from the vicinity of the well, and a third average measurement was observed. The difference between the three measurements was calculated to evaluate the sensitivity of the installation and to observe hysteretic effects from loading.

A preliminary estimate of the elastic modulus of the soil was performed by observing the displacement response to a vehicle parked at measured intervals from the installation. As in the qualitative experiment, a vehicle of known load was parked greater

than 75 m from the installation and a preliminary average measurement was observed as the displacement was sampled at 1 Hz. The vehicle was then parked for about 1 to 5 minutes adjacent to the borehole such that the front tires were approximately radially equidistant to the casing stickup and the back tires were similarly equidistant to the installation. The distance to one front tire and to one back tire was measured, and the average displacement was calculated for the time interval. The vehicle was then moved away from the borehole at an interval of about 3 m, and the measurement process was repeated until the difference between the most recent displacement measurement and the previous displacement measurement was approximately less than 10% of the displacement between the first and second displacement measurements. Once this had occurred, the vehicle was moved to greater than 50 m from the borehole, and a final displacement measurement was taken.

The displacement caused by the vehicle was determined as a function of radial distance and elastic modulus by assuming the subsurface is homogeneous and integrating the Boussinesq equation (Equation 2) numerically over the area of the four tires. The average displacement and load position were passed to the function in Appendix D to calculate the Young's modulus from the data. This function approximates a distributed load by summing the responses to a user-defined number of point loads over the loading area. The area over which the load acted was subdivided into a 1 x 1, 11 x 11, 101 x 101, and 1001 x 1001 cells, and the results from each trial were compared graphically to determine if the modulus estimate was converging. The modulus calculated using 1001^2

cells was taken as the final estimate for each loading position. The mean and 95% confidence interval were calculated from estimates of the modulus along each azimuth.

Precipitation Calibration

A running calibration of the soil modulus was performed by correlating precipitation measurements to corresponding displacement measured in the subsurface. This calibration was performed during each precipitation event by plotting the displacement measurements (sampled once per minute) that were sampled most nearly to the same time at which the precipitation measurements (sampled once every 5 minutes) were taken. This technique was applied to every rain event for which precipitation and displacement measurements were available, and the data were compiled into a single dataset. The calibration was performed using a linear regression passing through the origin. The calibration was bounded by calculating the 95% confidence interval of the slope.

2.7 Analysis

Data was processed using MATLAB scripts to correct and convert raw measurements into data vectors. These vectors were compiled to be compared for interpretation and application of further analyses. In some instances, additional corrections were applied to instruments that are sensitive to excitation voltage. Other datasets omitted segments of data containing responses to logged maintenance activities or shifted segments of data to align sequential datasets that were offset by adjustment of the instrument scale.

Data Processing

Data sets were separated into individual files based on the day they were collected, and these files were combined into a single compilation of all of the datasets using MATLAB scripts to adjust and combine the vectors. Borehole instrumentation data was collected on a different data acquisition system than weather data, the timestamps were converted to a common basis using units of days elapsed since the beginning of 2012. This eliminated problems comparing datasets sampled at different frequencies by different loggers. Segments of data were deleted to remove the effects of maintenance, calibration, equipment malfunction, and other factors. These activities were logged to ensure that *only* signal related to known sources is removed. Constant values were added to each displacement dataset to offset them to a common datum. This technique was used so displacements at the end of one dataset were consistent with values in the next dataset. The trend at the end of one dataset was extrapolated to beginning of the next dataset, and this trend was used to determine the offset value. This procedure reduces arbitrary steps in plots that contain multiple datasets. Compiled datasets were stored with omissions and offsets.

Filtering was used to clarify compiled datasets for graphs. Signal occurring over shorter time periods than the signal of interest was considered noise, and when the span of the noise exceeded one third of the magnitude of the signal of interest, the signal was filtered. The filtering method used was a moving average over a window centered on the sample. Uniform weighting was applied to the average for averaging windows of up to ten sampling periods, and normal distribution weighting with a standard deviation of 1/5

the averaging window was used for averaging windows of ten sampling periods or more. The averaging window was never allowed to exceed the time duration of the most rapid signal of interest.

Barometric Pressure Correction

Displacements caused by barometric pressure are spurious to the proposed application, and a model was developed and evaluated for removing these effects. This approach uses only measurements of barometric pressure to estimate the response of the soil.

The governing equation of the soil strain response to barometric loading is the diffusion equation under uniaxial strain. The diffusion equation for an irrotational displacement field is

$$\frac{\partial p}{\partial t} - c\frac{\partial^2 p}{\partial x^2} = -\frac{\eta}{GS}\frac{d\sigma_{xx}}{dt} \tag{12}$$

where p is the pressure field, t is time, η is the kinematic viscosity, G is the shear modulus, S is the storativity, σ_{xx} is stress acting in the x direction on an x-normal surface (such as the ground surface), and

$$c = \frac{\kappa}{S} = \frac{2\kappa G(1-\nu)(\nu_u - \nu)}{\alpha^2(1-2\nu)^2(1-\nu_u)} \tag{13}$$

where ν is the drained Poisson's ratio of the soil matrix, ν_u is the undrained Poisson's ratio of the soil matrix, and

$$\kappa = \frac{k}{\mu} \tag{14}$$

where k is the permeability and μ is the dynamic viscosity. The boundary value problem is the diffusion equation and the equilibrium equation

$$\frac{\partial \sigma_{xx}}{\partial x} = 0 \tag{15}$$

for all x and t. The boundaries are

$$\begin{aligned} &\sigma_{xx}(0,t) = -p_0(t) \\ &p(0,t) = p_0(t) \\ &\frac{\partial}{\partial x} p(L,t) = 0 \end{aligned} \tag{16}$$

for $t > 0$ where

$$p_0(t) \triangleq p(x = 0, t) \tag{17}$$

The initial condition for pressure is

$$p(x,0) = Ap_0(0) \tag{18}$$

where

$$A = \frac{\eta}{GS} \tag{19}$$

This condition is derived from the assumption that no diffusion occurs for time less than zero (i.e. Skempton's effect).

The solution to this problem for the displacement between two points in the subsurface is

$$\Delta U = -\Pi_0(\tau)\left(\xi_2 - \xi_1\right)\left(1-\alpha\right) + c\sum_{n=0}^{\infty}\left\{\left[\cos\left(w_1\right) - \cos\left(w_2\right)\right]\frac{\alpha_n(\tau)}{2n+1}\right\} \tag{20}$$

ΔU is the strain over the measured interval given by

$$\Delta U = \frac{\Delta u}{L} \tag{21}$$

where Δu is the displacement measured over interval L. $\Pi_0(\tau)$ is dimensionless pressure given by

$$\Pi_0(\tau) = \frac{p_0(\tau)}{p_m} \tag{22}$$

where $p_0(\tau)$ is atmospheric pressure and p_m is the characteristic pressure

$$p_m = \frac{E(1-\nu)}{2(1-2\nu)(1+\nu)} \tag{23}$$

The parameter α is the Biot-Willis coefficient, and

$$c = \frac{8\alpha\left(A-1\right)}{\pi^2} \tag{24}$$

$$w_i = \frac{\pi\xi_i(2n+1)}{2} \tag{25}$$

$$\alpha_n\left(\tau\right) = \frac{1}{2n+1}\left(\Pi_0\left(\tau\right) - \pi^2(2n+1)^2 I_0\left(\tau,n\right)\right) \tag{26}$$

where

$$I_0\left(\tau,n\right) = \begin{cases} \int_0^\tau \Pi_0\left(\tau-\tau'\right)e^{-\pi^2(2n+1)^2\tau'}d\tau', & n < \frac{1}{2}\left(\frac{1}{\pi}\sqrt{\frac{N}{\tau}} - 1\right) \\ \dfrac{\Pi_0\left(\tau\right)}{\pi^2\left(2n+1\right)^2} & \text{otherwise} \end{cases} \tag{27}$$

The dimensionless distance is

$$\xi_i = \frac{x_i}{L} \tag{28}$$

where x_i is the depth to anchor i from the ground surface. The dimensionless time is

$$\tau = \frac{t}{t_0} \tag{29}$$

where t is time and t_0 is the characteristic time given by

$$t_0 = \frac{4L^2}{D} \tag{30}$$

D is the pneumatic diffusivity of the soil, assumed to be

$$D = \frac{2kG\left(\nu_u - \nu\right)}{\alpha^2\left(1-2\nu\right)^2\left(1-\nu\right)\eta} \tag{31}$$

The barometric pressure time series as a function of dimensionless time is $P_0(\tau)$, and the dimensionless depth of the top and bottom anchors is given by ξ_1 and ξ_2 respectively. L is the thickness of the soil layer, and

$$A = \frac{\nu_u - \nu}{\alpha\left(1-2\nu\right)\left(1-\nu_u\right)} \tag{32}$$

Typical values for the parameters are given in Table 1.

Other Signal Correction and Filtering

Hydrological and geological events at the hours-to-days scale that influence the soil strain state may include semidiurnal and diurnal earth tides, diurnal barometric fluctuations, precipitation, and evapotranspiration. Earth tide effects, if any, will be isolated and removed using a spectral analysis of the data to identify tidal effects as in Acworth and Brain (2008). Weather measurements such as precipitation, pressure, and soil moisture on site provide a basis for comparison of the displacement signal to

hydrologic events and offer a means for separating measurement of hydrologic events from measurement of other events such as temperature variation and human activity.

Table 1. Parameters used in barometric correction analysis. These parameters are based on the geometry and geology of the Simpson Station site.

Parameter	Value	Units
α	1	-
G	15	MPa
ν	0.35	-
ν_u	0.4	-
k	10^{-14}	m^2
η	0.864	kg m^{-1} da^{-1}
D	2200	m^2 da^{-1}
A	0.28	-
L	33	m
x_1	6	m
x_2	7	m
ξ_1	0.18	-
ξ_2	0.195	-
t_0	1.68	da

Signal Comparison and Interpretation

The displacement measurements were compared with secondary on-site measurements by plotting sections of the datasets that occurred during the same time period and looking for corresponding changes in the datasets. When patterns emerged in the behavior of the two measurements, the signals were correlated as the change in displacement to the change in the secondary measurement. When the displacement signal could be predicted by the correlation curve and the secondary signal within the variability

of the correlation curve, the pattern became an interpretation of displacement signals showing the same behavior.

CHAPTER 3: RESULTS AND DISCUSSION

Field experiments demonstrated a clear, immediate response to point loading at both 2 and 6 m depth. The response to precipitation was more consistent and simpler to interpret at 6 m than at 2 m; consequently, experiments at the shallower depth were abandoned to pursue replication and comparison of behaviors for multiple devices installed at 6 m at the Simpson Station site. Though the responses of the different installations at this site to point and distributed loading were qualitatively consistent, they were different in magnitude and background signal and thus required correction for a more complete comparison.

Laboratory Experiments

Lab-Scale Response

Displacements were negligible after the first two increases in applied load, but then they responded abruptly as the load was changed (Figure 12). A displacement of 34 μm occurred after an increase in load of 10kPa (3.4 μm/kPa), and this was followed by a displacement of 70 μm following a load change of 37 kPa (2.1 μm/kPa). Those data were repeated with another increment of load and the experiment ended when the bladder burst. Displacement after the bladder burst occurred due to the rapid changes in load as the water infiltrated into the apparatus.

The results from this test demonstrate that the Sand-X is capable of measuring displacement in sand in response changes in surface loading. The response of the instrument to the last three loadings was immediate, and the last two responses were consistent. The magnitude of the response was evaluated by converting the compliance

given in parentheses above to Young's modulus. This was done by inverting the compliance and dividing by the distance between the anchors. This gives an estimate of Young's modulus of the sand on the order of 10^8 Pa. Values of the Young's modulus of sand range from 10^7 to 10^9 Pa (Albers, 2010; Rosenblad et al., 2010). This estimate, though it is probably unrealistic for the low confining stress in the test apparatus, is consistent with the literature and suggests that the instrument is working.

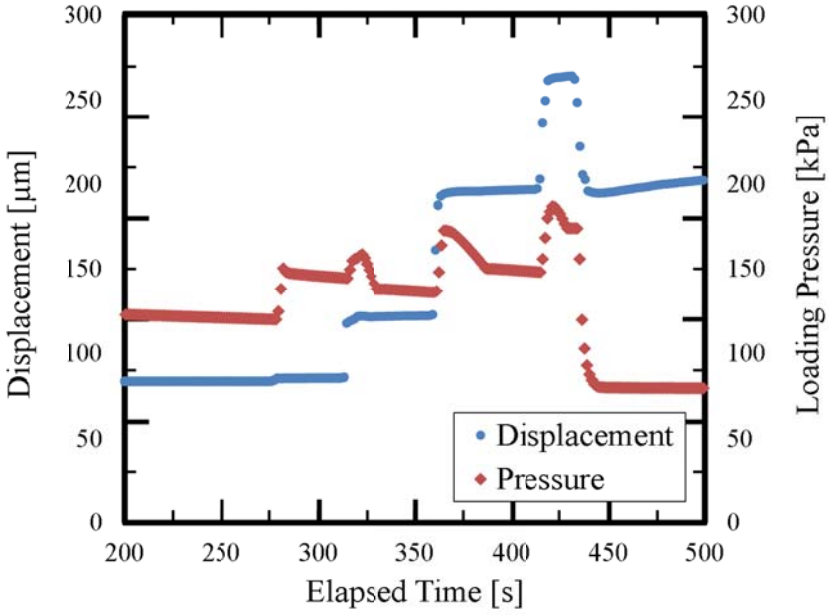

Figure 12. Displacement time series measured in a lab-scale apparatus with corresponding loading pressure.

Field Experiments

Field experiments were conducted at three sites, but tests at two sites were preliminary and the majority of the experiments were done at the Bull Test Farm site. The results include calibration data in response to point and distributed loads and analyses of

barometric effects. The main proof-of-concept data set was measured from February 2012 to August 2012 at the Bull Test Farm site.

The first fifteen weeks of data recorded by SX4 contained a continuous linear drift of 15.5 microns of compression per day after which the signal reversed naturally. This trend was removed from the data prior to all analyses.

Point-Load Response

Detailed response to point loads was used for calibration, and the scale of response was used to verify that the instrument was functioning correctly. The latter was an important tool during development, particularly early in the process when the initial

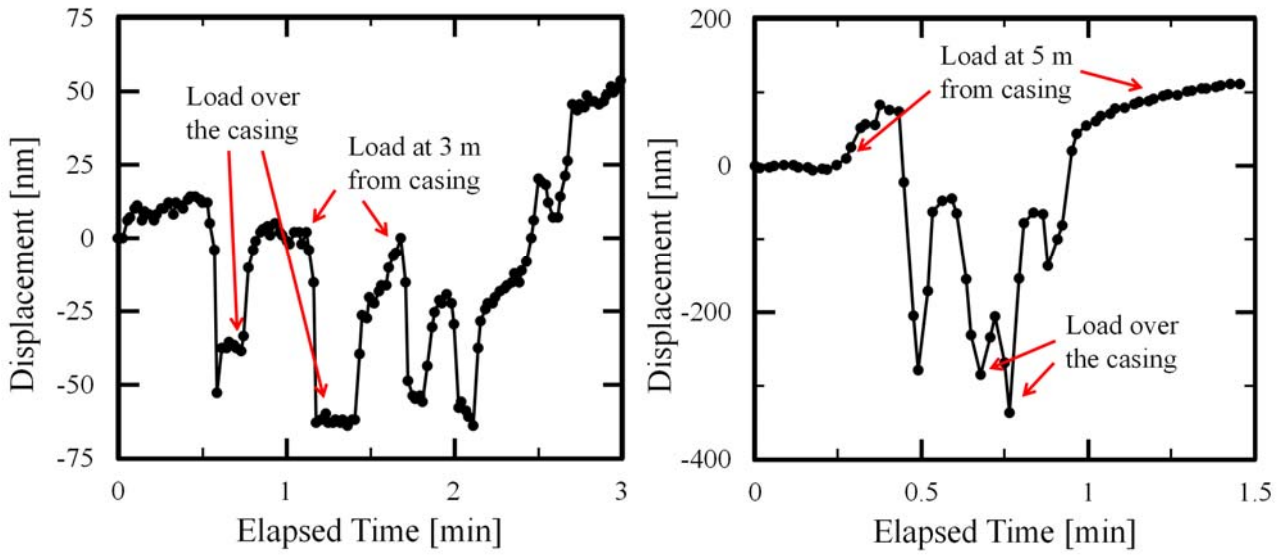

Figure 13. Response of Sand-X 1 to point loading. Loaded by the weight of a human (left). Loaded by the weight of a vehicle (right).

designs were being developed and proven. The first successful response was at Sand-X 1, when it responded to my weight (approximately 675 N) with a displacement of 50 nm and to a car (approximately 14,500 N) with a displacement of 350 nm. The functionality

of the device was further confirmed by alternating the position of the load from over the access casing to a distance of 3 to 5 m from the casing (Figure 13). The loads used in this test were distributed over 250 cm^2 (the area of my feet), so they were approximately point loads at the scale of several m. This experiment was the first demonstration of the expected response of the Sand-X in a field installation.

Sand-X 3, located at the Simpson Station site, responded to my weight with a displacement of 0.1 micron. A car approximately 3 m from the surface casing produced a displacement of 1.75 microns during initial verification testing. Sand-X 4 responded to my weight with a displacement of 0.4 micron and to a vehicle within 2 m of the access casing with a displacement 6.25 microns on average.

The simultaneous response of Sand-X 3 and Sand-X 4, which are separated by 24.5 m, was determined by slowly driving a vehicle back and forth between the two installations. Compression occurred when the vehicle approached, and extension occurred when the vehicle departed from the vicinity of a surface casing (Figure 15). During this experiment, Sand-X 4 compressed by 7.4 microns, but it only returned 6.3 microns. This hysteresis occurred once during the first loading/unloading cycle.

Young's modulus was estimated for Sand-X 3 to provide a preliminary calibration. Displacement was measured by Sand-X 3 as the location of the vehicle was varied along an azimuth of 100^o. The Young's modulus was calculated as a function of radial position of the applied load (Figure 14). Averaging along the azimuth gives a modulus of 6.5×10^7 Pa $\pm$ 4.1×10^7 Pa (uncertainty is 95% confidence interval). The results show that Young's Modulus calculated in this way is a strong function of the

radial distance of the load, varying by an order of magnitude over approximately 12 m (Figure 14). It is possible that the change in modulus is an artifact of the method of analysis. It is important to recognize that the analysis used to interpret the data (Equation 2) assumes the subsurface is homogeneous. As a result, it is unable to accurately predict properties in a heterogeneous setting, so Figure 14 should be regarded as a first approximation.

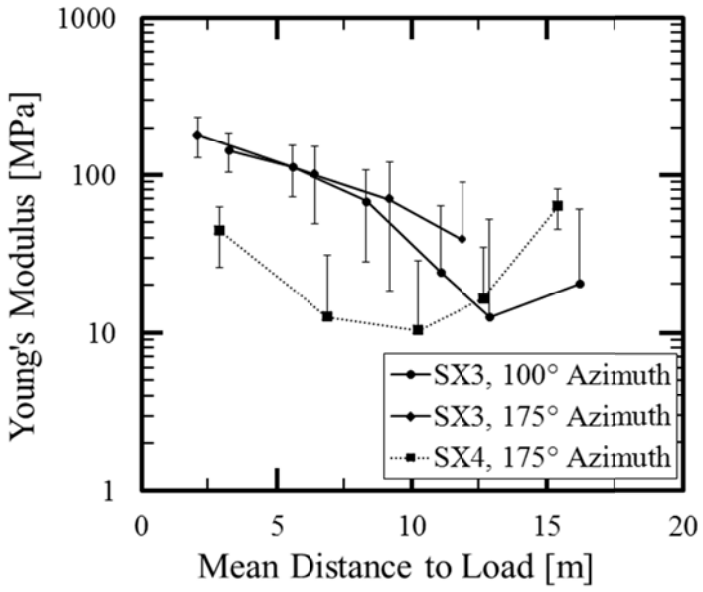

Figure 14. Young's modulus as a function of distance from the applied load to the access casing of SX3 and SX4 along two different azimuths.

Young's modulus was estimated for Sand-X 4 and Sand-X 3. The point load calibration experiment was repeated, varying the position of a vehicle along an azimuth of 175° from Sand-X 4 to Sand-X 3. The Young's modulus was calculated as a function of radial position (Figure 14). The average modulus from these results is 9.9×10^7 Pa ± 52×10^7 Pa for Sand-X 3 and 3.0×10^7 Pa ± 1.9×10^7 Pa for Sand-X 4 with uncertainty given by the 95% confidence interval of the population mean.

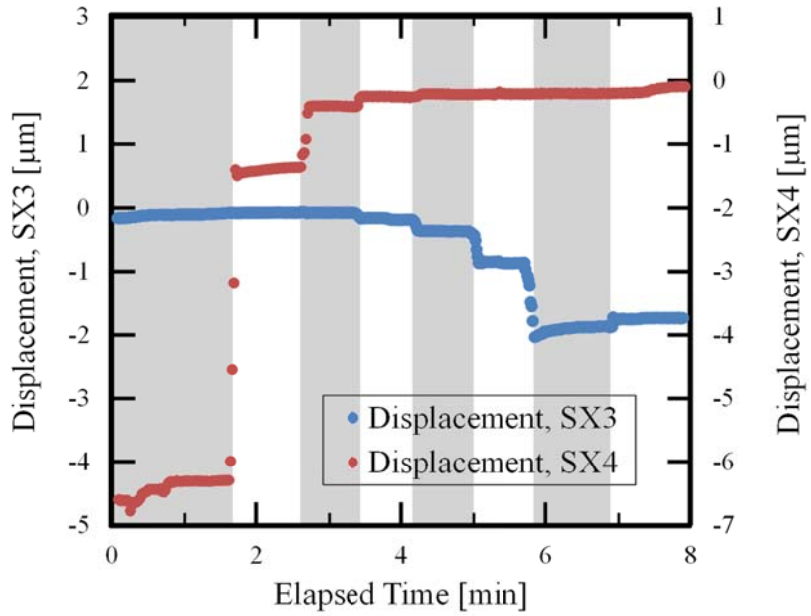

Figure 15 (above). Simultaneous calibration of Sand-X 3 and 4. Displacement measured by Sand-X 3 and 4 are shown on the left and right vertical axes and plotted in blue and red respectively. Time elapsed during the experiment is plotted on the horizontal axis. Alternating gray and white bars denote different loading positions.

Figure 16 (below). Point load calibration results for Sand-X 3 and 4. Displacement is plotted on the vertical axis, and the distance between the load and the access casing is plotted on the horizontal axis. The black bar indicates the approximate distance at which the soil no longer responded to the load.

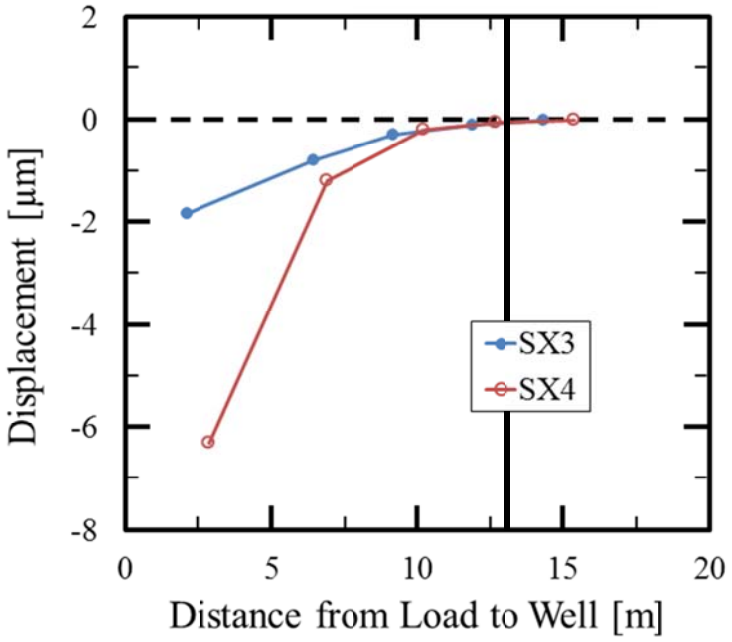

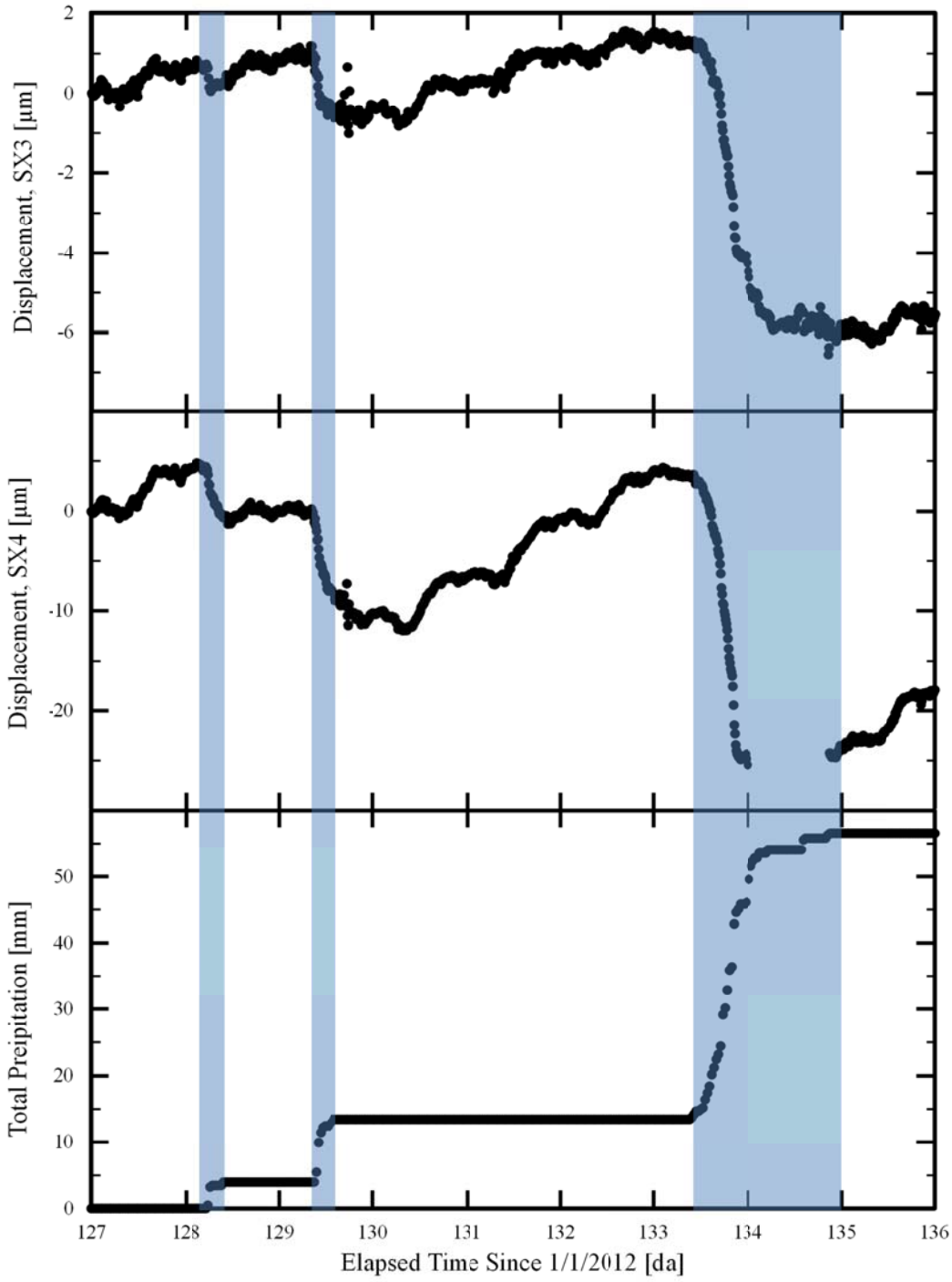

Figure 17. Sand-X 3 and 4 response during precipitation events of 5, 10, and 40 mm. Vertical axes are displacement measurements from Sand-X 3 and 4 and total precipitation from top to bottom, and the horizontal axis is elapsed time. Blue bands denote periods of precipitation.

For comparison, Young's Modulus was measured using soil samples from a pit approximatley 20 m from SX3 and SX4 (Murdoch *et al*., 2006). Those data indicate that the modulus increases from 2.4 x 10^7 Pa to 4.8 x 10^7 Pa as confining stress increases from 14 kPa to 140 kPa. The unit weight of the saprolite is approximately 15 kPa m^{-1}, so the Young's modulus is estimated to be 4.1 x 10^7 Pa.

Precipitation Response

Displacement and precipitation at the Simpson Station field site was measured at Sand-X 3 from January 2012 to September 2012 and at Sand-X 4 from April 2012 to September 2012. During this time there were approximately 40 rainfall events with a typical magnitude of 10 mm per event and a maximum of approximately 100 mm per event. The typical rainfall duration was 9 hours and the longest one was approximately 4 days.

The responses of SX3 and SX4 to precipitation were qualitatively similar but different in magnitude (Figure 17). The response to each precipitation event was immediate compression that continued for the duration of the event. The magnitude of the compression generally ranged from about 1 micron to 10 microns and correlated roughly to the magnitude of the precipitation event. Most precipitation events greater than 5 mm were identifiable in the displacement data. Instances where the precipitation was not evident in the displacement signal above background signal were presumably caused by large variations in barometric pressure during the rainfall event.

All rainfall events of 5mm or greater were compiled and used for calibration. This was done by pairing the cumulative rainfall of each event to the cumulative

displacement of each event and fitting the data from all events with a straight line (Figure 18). The calibration yields an average response of -0.16 µm displacement mm^{-1} rainfall ± 0.002 µm mm^{-1} with an R^2 of 0.95 for Sand-X 3 and -0.66 µm displacement mm^{-1} rainfall ± 0.069 µm mm^{-1} with an R^2 of 0.54 for Sand-X 4. The records from Sand-X 3 for one precipitation event, shown in gray

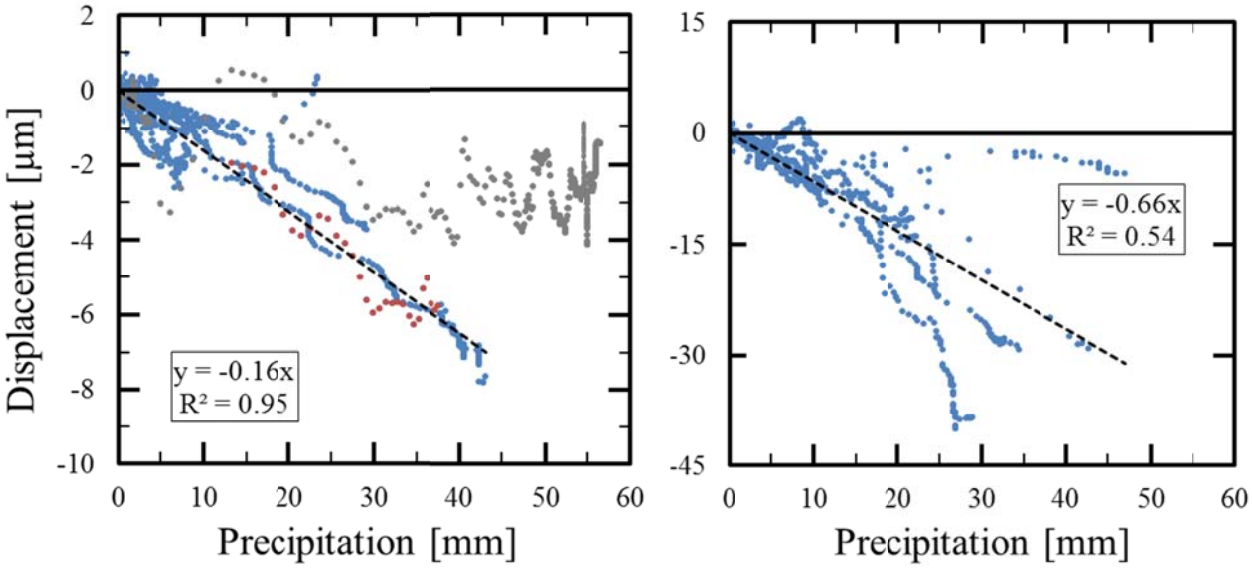

Figure 18. Precipitation calibration of Sand-X 3 and 4. Calibration of Sand-X 3 to precipitation (left). Calibration of Sand-X 4 to precipitation (right). Displacement is plotted on the vertical axes and cumulative precipitation is plotted on the horizontal axes. Blue data points denote data used in the calibration, gray data points denote data before correction, and red dots denote the corrected data, also used in the calibration.

in Figure 18, were anomalous during the early and late stages of the event, but a section of the event was observed to be consistent with the other data. The entire precipitation event was replaced with only the section that was consistent, shown in red in Figure 18, shifted by -2.5 µm to align it with the rest of the data. This corrected data was included during the calculation of the correlation factor.

Long-Term Behavior

Sand-X 3 measured alternating periods of compression and extension corresponding to measured precipitation and periods of no precipitation respectively. From the last week of January through the first week and a half of February, Sand-X 3 measured a net compression of nearly 10 microns distributed over three rain events (Figure 19). Following this was a period of about a month during which the net displacement remained relatively constant. Precipitation events occurring about one to two times every five days and corresponding to displacements of 2 to 3.5 microns were offset by soil expansion occurring between precipitation events. This period includes two gaps of 2 days or less, reducing the certainty of the long-term trend. From the second week of March to the third week of May, Sand-X 3 recorded a net soil expansion of nearly 20 microns. During this period, precipitation became heavier but occurred about once a week to once every 10 days. Corresponding soil compression ranged from 2.5 to 8 microns. This period began with a one week data gap and had a second gap of a day later on. The next month of data showed soil compression of about 20 to 30 microns with the uncertainty caused by a period of six days during what appears to be a reversal in the background trend (Figure 19). Compression ranging from 3 to 8 microns corresponds to three precipitation events on the order of 25 mm or more occurred during this period.

Displacement measurements were converted to changes in water content using the calibration factor determined through the correlation to rainfall. This calibration factor was assumed to be constant over the time period. This reveals a seasonal fluctuation with an increase of nearly 40 mm of soil water loading during the first month followed by a

net loss of 90 mm of water loading over the subsequent two and a half months (Figure 20). Daily averages of water content change show a net loss of water during most days with a periodic net increase during rainy days. The time derivative of water volume per unit area was interpreted as the vertical flux out of the region sampled by the instrument (Figure 19).

It is also possible that displacements may be caused by horizontal flow of water, and so the expression of the unloading rate as a vertical flux using the correlation factor will be an upper limit of the vertical flux. The ground slope at the site of Sand-X 3 is a 2% grade sloping downward to the NE, and it is covered in grass, so the overland flow is expected to be small in most cases. Lateral flow on the top of the B horizon may occur in some cases, but it is expected to be small. It follows that the temporal derivative of the water volume per unit area is the vertical flux into, or out of, the averaging volume.

Vertical fluxes estimated using displacement data were compiled and plotted as a function of time with the sum of ET estimated using the monthly average pan evaporation (Purvis, 2010) and recharge for these months in 2012 estimated using hydrograph data for a nearby stream. The estimates from the displacement data of monthly water loss were 3.9 cm, 9.7 cm, 8.0 cm, and 5.3 cm for the months of February through May respectively. The evapotranspiration estimate was determined by multiplying the pan evaporation by the crop factor for fescue grass, 0.8 (Hargreaves, 1974). This gives net evaporation of approximately 5 cm during February which increases progressively to approximately 13 cm in May (Figure 20). The recharge for this period decreases from 2.5 cm in February to 0.5 cm in May. The total water loss from land pan and hydrograph data is 7.2 cm 10.2

cm, 12.1 cm, and 13.1 cm for February through May. The net evapotranspiration and recharge estimated from land pan measurements and hydrograph data respectively was 43 cm with a standard deviation of 14.9 cm, and the net soil water loss estimated from displacement measurements was 27 cm with a 95% confidence interval of ±6.7 cm. The data show consistency during March and April, but the results from February and May are inconsistent. This is likely a result of the use of historic pan data in combination with the difference in scale between the hydrograph recharge estimate (approximately 250 km^2) and the Sand-X measurement scale (approximately 500 m^2).

Barometric Response

The typical response of both Sand-X 3 and Sand-X 4 to barometric fluctuation is compression during positive pressure change and extension during negative pressure change. This occurred over a range of time scales, but there is a significant variation on a diurnal scale in both Sand-X 3 and Sand-X 4. The magnitude of the diurnal displacements in Sand-X 3 is 0.5 to 1 microns (Figure 22), whereas it is 4 to 6 microns in Sand-X 4. The barometric pressure changed by 200 Pa to 400 Pa on a diurnal cycle during the study. The barometric pressure changed by 200 Pa to 400 Pa on a diurnal cycle

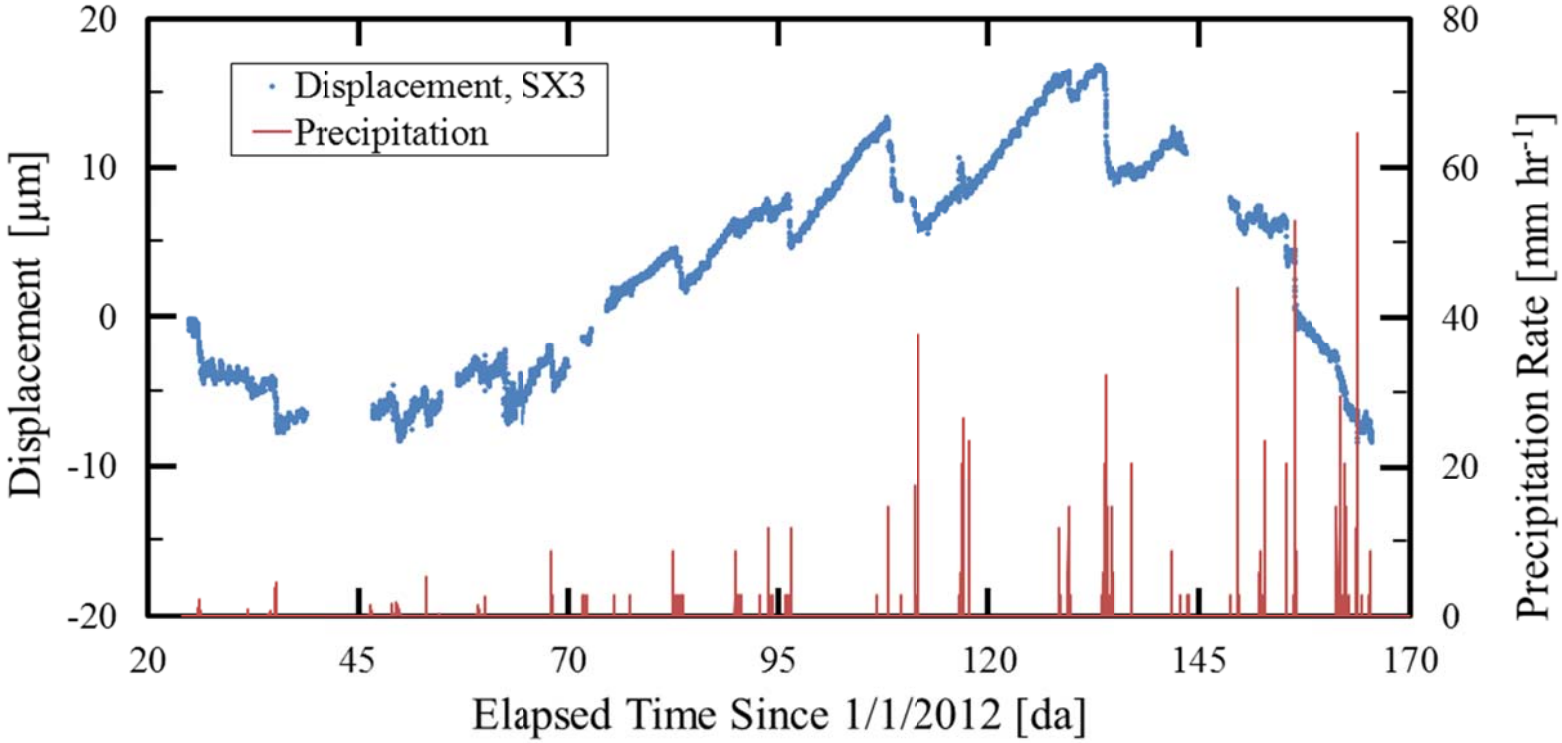

Figure 19. Displacement record of Sand-X 3 compared to precipitation rate from late January 2012 to late June 2012. Left and right vertical axes are displacement and precipitation rate respectively, and the horizontal axis is elapsed time. The blue data points are displacement and the red line is precipitation rate.

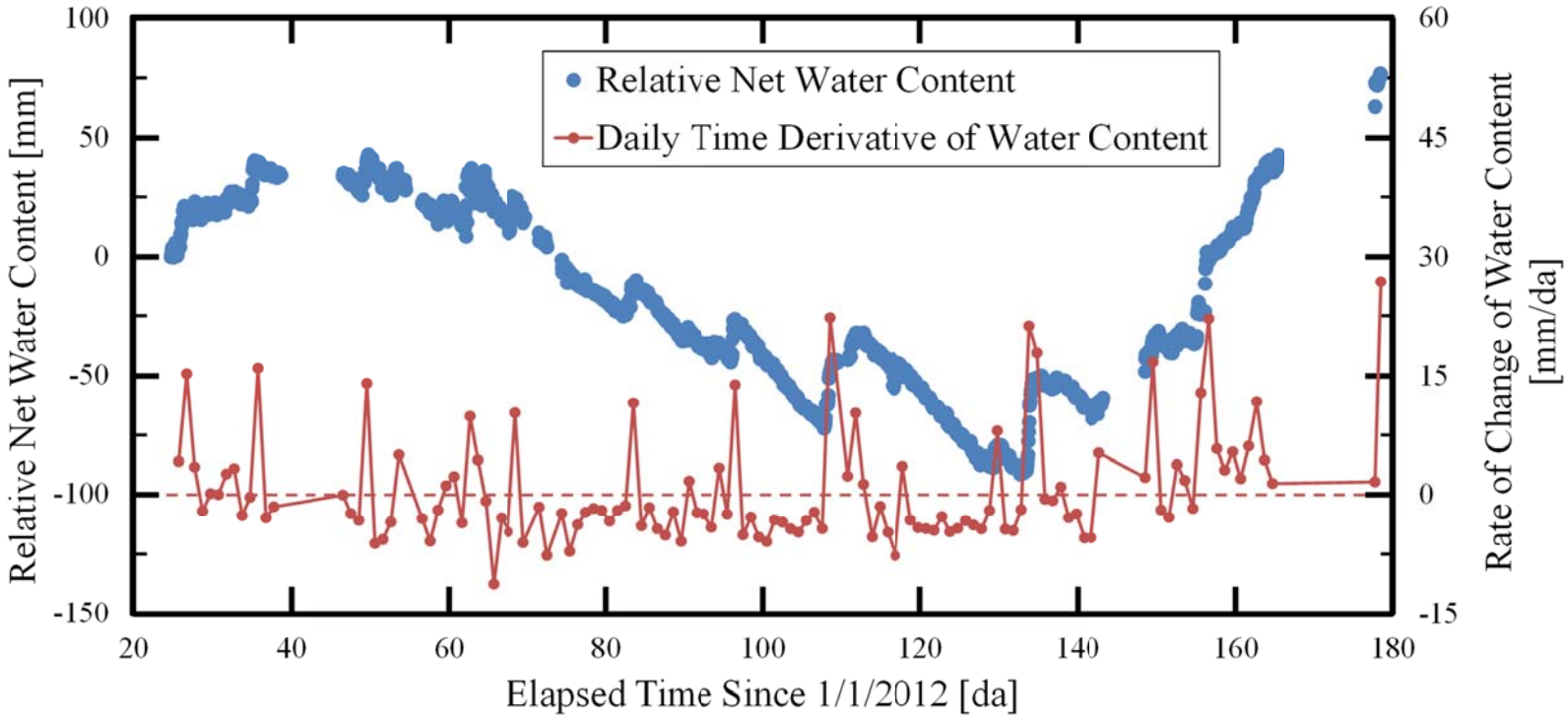

Figure 20. Interpretation of displacement as change in soil water. Soil water volume estimated from displacement data using precipitation calibration (blue). Daily time derivative of the water content (red).

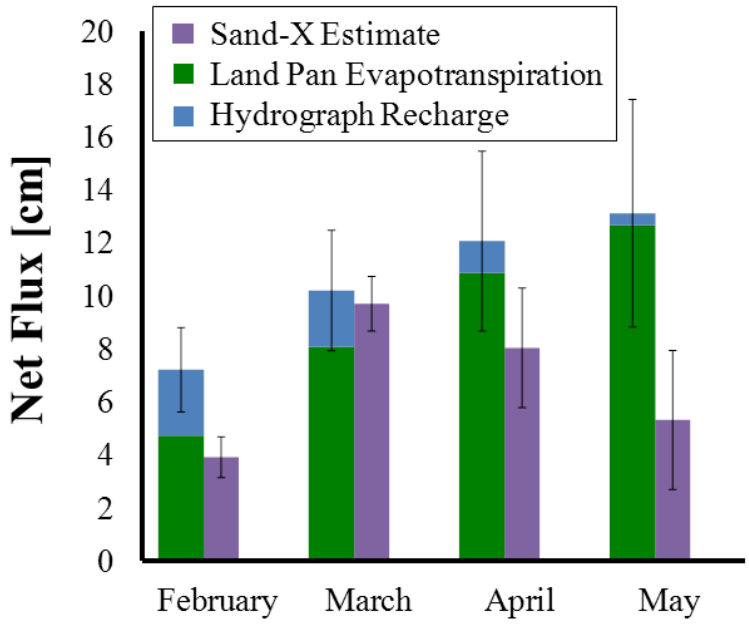

Figure 21. Monthly totals of inferred water loss compared to totals of evapotranspiration and recharge. The vertical axis is the net water flux, and the horizontal axis is the month over which water flux totals were taken. The purple bars are water flux estimates from Sand-X 3, the green bars are estimates of evapotranspiration from historical land pan measurements, and the blue bars are estimates of recharge from hydrograph data.

during the study. The largest diurnal changes in barometric pressure occurred predominantly during roughly 8 hours centered on noon, with the morning hours characterized by increasing pressure that peaks slightly before noon and is followed by sharp drops in pressure during the afternoon. The pressure was relatively stable at night (Figure 22).

The displacement appears to follow the barometric trend, with compression in the morning followed by abrupt expansion that starts with the drop in barometric pressure slightly before noon. The displacement trend reverses with compression that starts in the late afternoon just as the barometric pressure stabilizes for the night (Figure 22). The

displacement follows an expected response to barometric loading, although the timing of the change is unexpected. In most cases, a reversal in the displacement trend precedes a reversal in the barometric pressure by roughly an hour (Figure 22). In other places in the time series, the reversals occur at roughly the same time. During these periods, the magnitude of the diurnal displacement signal is generally 0.5 microns, smaller than that shown in Figure 22.

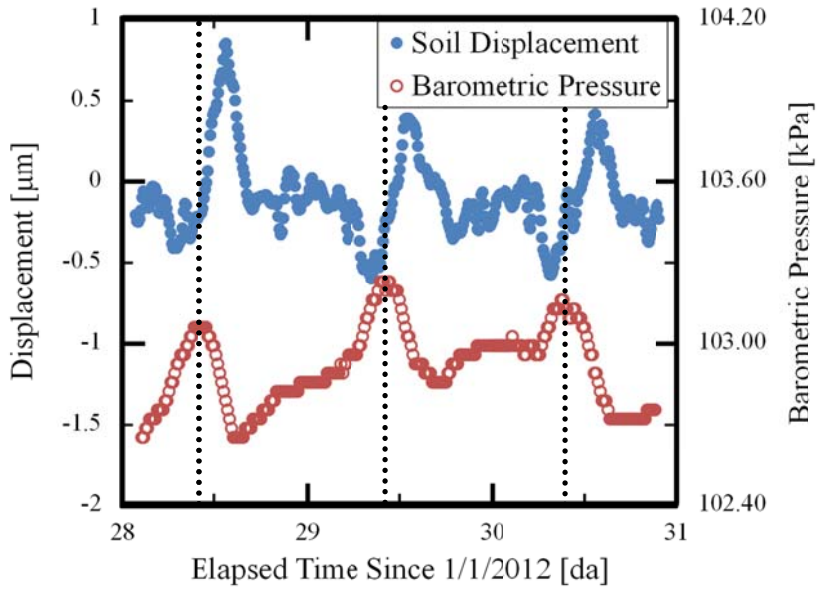

Figure 22. Displacement and barometric pressure as functions of time. Displacement follows most changes in barometric pressure. Dotted lines indicate peak daily pressure.

The diffusivity of the soil controls the rate at which the pore pressure equilibrates with the surface pressure, and consequently barometric change that occurs relatively slowly compared to the diffusivity will have less effect than barometric change that occurs relatively quickly. This property is a nonlinear function of the unsaturated soil moisture, and consequently it can vary dramatically in ways that are difficult to predict.

This property affects the magnitude and timing of the response of the soil to barometric loading, and it is possible that variation in diffusivity is the reason for changes in the peak offset between the displacement and barometric signals.

A month of data from early October 2012 demonstrates the performance of the barometric correction during three rain events. The first precipitation event occurred on day 272 and was 1 mm in magnitude; the second event occurred on day 274 and was about 80 mm in magnitude; and the third precipitation event occurred on day 288 and was about 10 mm in magnitude. The uncorrected response to these events was indiscernible from the background barometric fluctuation, 21 μm, and 3 μm respectively (Figure 23). After correction, the first precipitation event became visible but still difficult to quantify , 21 μm, and 2.5 μm respectively. During periods between the precipitation events, the uncorrected data is consistently linear over timescales of days to weeks. During these same periods, the corrected data is approximately piecewise quadratic corresponding to barometric fluctuation on the timescale of 3 to 5 days to which the uncorrected data was insensitive.

From these results, the correction appears to have a greater effect on smaller displacements than it does on large displacements. This is consistent with the expected results of the analysis. The introduction of fluctuations over several days was undesirable because the observed displacement response seemed to be somewhat more closely correlated to the rate of change of barometric pressure rather than the magnitude of the barometric pressure change. This result is likely a consequence of a poorly defined

pneumatic diffusivity which limits the response of the soil to barometric pressure signals at longer time intervals.

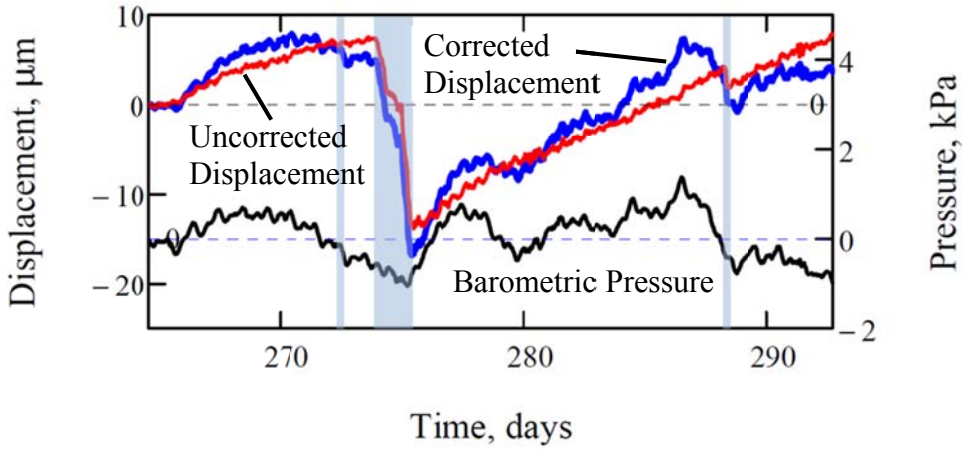

Figure 23. Demonstration of the barometric correction technique. Shaded regions indicate the occurrence of precipitation.

Discussion

Implications

The sensitivity of displacement measurements at depth to change in surface load resulting from hydrologic events demonstrates the feasibility of this technique for characterizing the hydrology. The lab-scale experiments indicate that the Sand-X is sensitive to load change in sand. The stiffness of soils *in situ* ranges from 10^6 Pa to 10^8 Pa (e.g. Albers, 2010; Ng and Leung, 2007; Das, 2006) which gives a theoretical displacement of 10^{-8} to 10^{-6} m during a 0.1 mm rainfall over a 1-m interval using Equation 9. These displacements are measurable with high-resolution transducers.

The averaging volume of the Sand-X encompasses the soil at depth and extends to the ground surface such that load changes at depth, near the surface, and acting on the

surface influence the measurement. As a result, this technique is complementary to established and evaluation-stage techniques for estimating soil moisture and near-surface fluxes which average near the surface (Entekhabi *et al*., 2004; Shuttleworth *et al*., 2010). A water balance of the soil between the Sand-X and the ground surface can be separated into its component fluxes and storage using concurrent measurements of displacement at depth and near-surface moisture and fluxes. This approach could yield a method for inferring processes such as ponding and recharge directly.

The scalability of the averaging region offers flexibility of measurement that is atypical for *in situ* techniques of measuring soil moisture. A challenge of upscaling techniques is accounting for the effect of variability on different scales of measurement. This is a particular problem for calibrating measurements of soil moisture observed by satellites. Installations of Sand-Xs at multiple depths at a single site would measure soil loading change at different scales and would provide a basis for comparison of the variability at multiple scales and its effect on the accuracy of upscaling techniques.

Limitations

The sensitivity of the soil to loading beyond the scope of hydrologic processes results in spurious signals superimposed on the hydrologic signal. Diurnal barometric fluctuations cause continuous deformation of the soil which must be removed to maximize the resolution of hydrologic measurements. Anthropogenic activity, the presence of large animals such as cattle, and ecological changes are sources of spurious signal that are more difficult to predict. Installations that are susceptible to these factors

will require case-by-case evaluations to determine the impact of and methods to remove these factors.

The soil stiffness controls the displacement and consequently limits the applicability of the Sand-X. The minimum theoretical resolvable load is

$$W_{res} = \frac{\delta_{res} E}{L} \tag{33}$$

where δ_{res} is the resolution of the transducer, E is the modulus of the soil, and L is the distance between the anchors. The smallest resolvable load ranges from 10^{-2} Pa to 1 Pa for a modulus ranging from 10^{6} Pa to 10^{8} Pa, an instrument resolution of 10^{-8} m, and an anchor spacing of 1 m.

Broader Impacts and Contexts

It may be possible to use measurement of displacement at depth to estimate the carbon balance of a forest. Fire, insect- or blight-induced mortality, and growth of plant matter results in load change. These changes are a consequence of the sequestering or liberation of carbon and can be used to estimate the resulting change in carbon storage (e.g. Chen *et al*., 2000). In the case of forest fire, the release of carbon is estimated to be on the order of kilograms per square meter, but making accurate estimates of this release remains a challenge (Wong, 1978). With the level of global interest on climate change studies, the ability to measure these changes directly at the scale of hectares provides the possibility for understanding how the carbon balance changes in a natural setting.

CHAPTER 4: CONCLUSIONS

The Sand-X revealed patterns suggestive of evaporation and seasonal change in soil moisture and showed clear, consistent responses to precipitation and point loading. Interference from barometric pressure was evident in the signal, but a model of the response of soil displacement to barometric pressure shows promise as a tool for removing these effects. Temperature change corresponded to change in displacement following emplacement of the transducer at depth, but it did not have measurable effect on the displacement during extended operation.

4.1 Major Findings

The hypothesis that displacement at depth could be used to measure change in soil moisture at the surface was confirmed. Not only did the Sand-X respond distinctly to moderate-to-large precipitation events, it measured a response between these events that is commensurate with the sum of evapotranspiration and recharge in the vicinity of Clemson, SC. The theoretical resolution of the instrument, which depends on the stiffness of the soil in which it is emplaced, is on the order of 1 Pa in the stiffest soils, equivalent to a resolution of 0.1 mm of water loading. This is comparable to the resolution of commercially-available precipitation gauges and soil moisture probes. The greatest limitation to the resolution of the displacement measurements is the response of the soil to barometric loading which fluctuates by hundreds of Pascals per day.

The response to precipitation events was clear and consistent. A correlation of the displacement to the load change suggested that Sand-X 3 responded measurably to

distributed load changes on the order of 0.25 mm, but spurious signal introduced by barometric pressure obscured signal at this level. The correlation between displacement and precipitation provided a calibration for converting displacement at depth to equivalent change in soil water.

Measurements of displacement over months interpreted as change in soil water indicated a trend suggestive of decreasing moisture content interpreted as the combined effects of evaporation and recharge. Translating displacement to change in soil moisture using the correlation of displacement to precipitation allowed the loss of soil moisture to be quantified. These estimates of daily evaporation and recharge averaged over each month showed estimates that followed the trend of historic averages of evapotranspiration estimates from pan evaporation. Subtracting the historic estimates of ET from the decreasing moisture measurements yielded an estimate of recharge integrated over five months that was consistent with the value in the literature for the upstate of SC.

The response of all of the installations to point loading was consistent with the behavior predicted by the Boussinesq equation for vertical displacement (Equation 2). This consistency indicates that measurements of the point load magnitude and the distance from the point load to the access casing can be used to estimate the elastic modulus of the solid skeleton. Variation in the estimates of the modulus suggested that the system was not homogeneous as assumed. Likewise, a calibration along a different radial path yielded a smaller extent of measurement, indicating that the measurement region is not circular as it would be in a homogeneous system.

The theoretical resolution of the displacement response is proportional to the resolution of the transducer and the stiffness of the soil skeleton and inversely proportional to the length of the measurement interval. The current system, with a resolution of 10^{-8} m and measurement interval of 1 m, is theoretically capable of measuring distributed load change of as little as 1 Pa in stiff soils with a modulus on the order of 10^{8} Pa. Consequently, the Sand-X is expected to perform well even in the most limiting soils.

Barometric pressure introduces a signal that typically exceeds 0.5 μm da^{-1} which is sufficient to obscure the response of the soil to evaporation, recharge, and precipitation events smaller than 5 mm. The barometric-corrected displacement was of marginally sufficient quality to reveal precipitation events of 1 mm that were obscured in the uncorrected signal. By using a field-estimated pneumatic diffusivity, it should be possible to improve these results. This approach is not yet refined, but it shows promise as a simple method for correcting the effects of barometric loading.

4.2 Closing Remarks

The Sand Extensometer shows promise as a tool for estimating soil moisture. The displacement at depth is sensitive to load change at the surface over a region that scales as approximately twice the depth of installation and is well-suited to measuring distributed changes in load such as variation in soil moisture. As a hydrologic tool, this method provides a way to measure soil moisture change at an important scale for hydrologic problems and makes it possible to examine the effect of scale of measurement on resolving the variability in soil moisture. This method has the additional advantage of

being sensitive to soil moisture at depth which makes this approach complementary to techniques that measure near the ground surface. Its sensitivity to both point and distributed loading suggests that the opportunities for future research using this technique span the fields of hydrology, climatology, ecology, glaciology, and many more.

APPENDICES

Appendix A

Electronics and Specifications

Device	Description	Full Scale	Accuracy	Resolution	Manufacturer	Supply Voltage [V]	Peak Power Consumption [mW]
DVRT & DEMOD	Displacement transducer and demodulator	500 µm	±0.1%	10 nm*	MicroStrain	9	352
SER1CH-UA	24-bit analog-to-digital converter	0 - 5 V Input	-	3×10^{-7} V	Symmetric Research	9	10.8
MMB26V5M2B0T3A8CE	Barometric pressure transducer	88 - 108 kPa	±0.05%	< 1 Pa	Omegadyne, Inc.	12	1500
CR800	Datalogger, 13-bit analog-to-digital converter	-5 to 5 or 0 - 5 V	-	6×10^{-4} V	Campbell Scientific	12	16
PX138	Differential pressure transducer, ±1 psi	-6.9 to 6.9 kPa	±0.1%	30 Pa*	Omega	9	32
LM35 TO-46	Temperature sensor	0 - 100 C	0.5°C	< 0.01°C*		9	1.8

* Indicates the resolution was observed in practice.

Appendix B

CRBasic Data Acquisition Program

```
'CR800 Datalogger
'date: 2/23/12
'program author: Clay Freeman

''''''''''''''''''''''''''''''''''''''''''''''''''''''''''''''''''''''''''''''''''''''
' WIRING INSTRUCTIONS
' It is possible to connect and log data from up to two Symmetric
Research 24-bit
' A/D boards simultaneously; this code demonstrates how this would be
done. To log data from
' two boards, connect the RTS and DTR pins from BOTH boards into the C1
and C2 ports and wire
' the SDO outputs To C3 and C4 as indicated below.

' LTC A/D Serial Campbell Pin
' ------- ------ ------------
' CS    RTS   C1
' SCK    DTR   C2
' SDO (1)  CTS   C3
' SDO (2)  CTS   C4

' DECLARE STORED VARIABLES
Public batt_volt, PTemp, Err1, Err2, DataCounts1 As Float, DataCounts2
As Float, DiffP1 As Float
Public DiffP2 As Float, BaroP As Float, WellTemp1 As Float, WellTemp2
As Float
Public V1 As Float, V2 As Float, bithist1(5) As Float, bithist2(5) As
Float, bitdiff1(4) As Float
Public bitdiff2(4) As Float, SpcCnt As Long = 0

' DECLARE SHARED VARIABLES
Public BinOut1(32), BinOut2(32), i, BinVal, PinIdx, Val, DV, Err, DVRT
Public arr(N) As Float, dev As Float, cnt As Long, currval As Float,
TotIter As Long = 1


''''''''''''''''''''''''''''''''''''''''''''''''''''''''''''''''''''''''''''''''''''''
' Define data table
''''''''''''''''''''''''''''''''''''''''''''''''''''''''''''''''''''''''''''''''''''''

DataTable (SXDATA,1,-1)
      DataInterval (0,1,Min,0)

      ' Internal measurements
      Minimum (1,batt_volt,FP2,0,False)
      Sample (1,PTemp,FP2)

 ' External measurements
 Average (1, V1, Float,false)
```

```
 Average (1, V2,Float,false)
 Sample (1, Err,UINT2)
 Average (1,DiffP1, IEEE4, False)
 Average (1, DiffP2, IEEE4, False)
 Average (1, BaroP, IEEE4, False)
 Average (1, WellTemp1, IEEE4, False)
 Average (1, WellTemp2, IEEE4, False)
EndTable


''''''''''''''''''''''''''''''''''''''''''''''''''''''''''''''''''''''''''''''''
' Low level, LTC2400 A/D controls and functions
''''''''''''''''''''''''''''''''''''''''''''''''''''''''''''''''''''''''''''''''
Sub SetSCK(Val)
 PortSet(2,Val)
EndSub

Sub SetCS(Val)
 ' Note that the chip select pin is active LOW rather than HIGH. The
code has been corrected
 ' to reflect this characteristic.
 PortSet(1,Val)
EndSub

Function GetSDO(Pin)
 If Pin = 3
  ReadIO(BinVal,&B0100)
  If BinVal < 0
   Err = -2
   ExitFunction
  EndIf
  Return(BinVal)
 ElseIf Pin = 4
  ReadIO(BinVal,&B1000)
  If BinVal < 0
   Err = -2
   ExitFunction
  EndIf
  Return(BinVal)
 EndIf
EndFunction


''''''''''''''''''''''''''''''''''''''''''''''''''''''''''''''''''''''''''''''''
' Ser1ch subroutines and functions
''''''''''''''''''''''''''''''''''''''''''''''''''''''''''''''''''''''''''''''''

Sub AtoDInit()
 ' The A/D is initialized by setting chip operation to "external clock"
mode
 ' "External clock" mode is selected when SCK is low on the falling
edge of CS.

 Call SetSCK(0) ' Set SCK to low before lowering CS
```

```
 Call SetCS(0)  ' Guarantee that CS falls by making sure it starts high
 Call SetCS(1)  ' Lower CS to select "external clock" mode
 Call SetCS(0)  ' Put A/D chip to sleep

EndSub


' Check A/D to make sure it is ready for output
Sub AtoDRequest()

 Call SetCS(1) ' Wake up A/D chip
 Call SetSCK(1) ' Open output window to verify that end of conversion
occurs
 Call SetSCK(0) ' Close output window
 Call SetCS(0) ' Begin new conversion and put A/D chip to sleep

EndSub


' Wait for A/D to end conversion before dumping bits from the chip
Public EOC, MaxCounts, Count

Sub AtoDWaitForReady()
  MaxCounts = 5000

 DV = GetSDO(3)
 Call SetCS(1) ' End conversion; wake up A/D

 ' Check For SDO low, indicating end of conversion
 EOC = 1
 Count = 0
 While EOC >= 1
  EOC = GetSDO(3)
  Count = Count + 1

  If Count > MaxCounts Then
   Err = -1
   DVRT = -1
   ExitSub
  EndIf
 Wend

EndSub


' Dump bits from A/D chip
Public LastCnt, Pin1, Pin2

Sub AtoDRead(Pin1, Pin2)
LastCnt = 1

 For i = 32 To LastCnt Step -1
  Call SetSCK(1)
  BinOut1(i) = GetSDO(Pin1)/(2^(Pin1-1))
```

```
  BinOut2(i) = GetSDO(Pin2)/(2^(Pin2-1))
  ' DV = DV + 1 ========= Debugging term

  Call SetSCK(0)
 Next


EndSub


''''''''''''''''''''''''''''''''''''''''''''''''''''''''''''''''''''''''''''''''
' Data Processing Functions
''''''''''''''''''''''''''''''''''''''''''''''''''''''''''''''''''''''''''''''''

Public Sig1 As Long, Exr1 As Long, Sig2 As Long, Exr2 As Long
Sub SplitBinVal()
' This function serves three roles:
'  1. It splits the decimal array representing a binary number into its
       component variables
'  2. It converts the binary number representing the data point into
       decimal counts
'  3. It checks the input voltage indicators Sig (sign) and Exr
       (extended input range) to verify that the voltage input falls
       on scale and throws an error if it does not

 For i = 5 To 28
  DataCounts1 = DataCounts1 + BinOut1(i)*2^(i-5)
  DataCounts2 = DataCounts2 + BinOut2(i)*2^(i-5)
 Next

 Exr1 = BinOut1(29)
 Sig1 = BinOut1(30)

 Exr2 = BinOut2(29)
 Sig2 = BinOut2(30)

 If Exr1 = 1
  If Sig1 = 1
   Err1 = -3
  Else
   Err1 = -4
  EndIf
 EndIf

 For i = 1 To 32
  BinOut1(i) = 0
  BinOut2(i) = 0
 Next

 'Return(DataCounts1, DataCounts2)
EndSub

Sub ResetValues()
 DataCounts1 = 0
```

```
 DataCounts2 = 0
 'DVRT = 0
 'Err = 0
EndSub

'''''''''''''''''''''''''''''''''''''''''''''''''''''''''''''''''''''''''''''''''
' Main Program
'''''''''''''''''''''''''''''''''''''''''''''''''''''''''''''''''''''''''''''''''

BeginProg
 Scan (1,Sec,0,0)
            PanelTemp (PTemp,250)
            Battery (batt_volt)

            VoltSe(DiffP1,1,mV5000,1,True,0,_60Hz,1,0)
            VoltSe(DiffP2,1,mV5000,2,True,0,_60Hz,1,0)

            VoltSe(WellTemp1,1,mV250,3,True,0,_60Hz,1,0)
            VoltSe(WellTemp2,1,mV250,4,True,0,_60Hz,1,0)

  VoltSe(BaroP,1,mV5000,5,True,0,_60Hz,1,0)

  Call AtoDInit()
  Call AtoDRequest()
  Call AtoDWaitForReady()
  Call AtoDRead(3,4)

  Call SplitBinVal()
  V1 = DataCounts1*(2.96*10^(-7))
  V2 = DataCounts2*(2.96*10^(-7))

  CallTable SXDATA

  Call ResetValues()
      NextScan
EndProg
```

Appendix C

MATLAB Data Processing Routine

```
function ProcessData(FileDate)

% Collect user-specified files for processing
files = dir(strcat(pwd,'\',FileDate,'*.csv'));

% Identify and assign file names for different datasets
SXfn = ''; Wfn = ''; Tfn = '';SMfn = '';
for i = 1:length(files)
  if strfind(files(i).name,'SX')
    SXfn = files(i).name;
  elseif strfind(files(i).name,'Weather')
    Wfn = files(i).name;
  elseif strfind(files(i).name,'T');
    Tfn = files(i).name;
  elseif strfind(files(i).name,'SM');
    SMfn = files(i).name;
  end
end

% Determine which files were not available and print this info in a
message
msgstr = {'' '' ''};
msg = zeros(3,1);
if strcmp(SXfn,'');msgstr{1} = 'Sand-X'; msg(1) = 1;end
if strcmp(Wfn,''); msgstr{2}= 'Weather'; msg(2) = 1; end
if strcmp(SMfn,''); msgstr{3} = 'Soil moisture'; msg(3) = 1; end

if any(msg)
  msgout = 'The following data could not be
found:\n%15s\n%15s\n%15s\n';
  fprintf(msgout,msgstr{1},msgstr{2},msgstr{3});
end

% Call data-processing functions
if msg
  fprintf('No Data was found.\n');
  return
end
if ~msg(1)
  [t,x1,DiffP1,Twell1,x2,DiffP2,Twell2,BaroP,BattV] = CSdump(SXfn);
end
if ~msg(2)
  [tW, v,vmax,vdir,R,P,totP,RH,WTemp,tT,T] = HOBOdump(Wfn,Tfn);
end
if ~msg(3)
  [tSM, SM] = SMdump(SMfn);
end
```

```
% Create meta data variable
load('Bull_Test_Meta.mat')
meta_data.TSi{1} = t(1);
meta_data.TSf{1} = t(length(t));

% Store data
clear files i SXfn Wfn Tfn msgstr msg
save(strcat(FileDate,'.mat'));

% Make data available to user
%vars = who;
%for i = 1:length(vars)
%  if ~strcmp(vars(i),'vars');assignin('caller',vars(i),);end
%end

end

function [t,x1,DiffP1,Twell1,x2,DiffP2,Twell2,BaroP,BattV] = CSdump(fn)
% Function: DumpCSData
% Author: Clay Freeman
% Date Created: 3/6/2012
% Date Modified: 4/25/2012
%
% This function takes the data file specified by input variable 'fn,'
% collects the displacement, differential and barometric pressure, well
% temperature, battery voltage, and any error messages that occurred
during
% collection and outputs them for processing. Additionally, the
function
% writes a '*.mat' file--a MATLAB data file that is very fast and easy
to
% open--with the filename specified by the variable 'fo'.
%
% Input Variables:
% fn (filename) - a string value...e.g. fn = '12-3.6 - Sand-X 3.csv'
% fo (file out) - a string value...e.g. fo = 'Sand-X 3 Dumped Data.mat'
%
% UPDATES:
% 1. Requires that the SX dataset have ONLY one header row
% 2. With (1.), function is able to determine the correct column for
each
% dataset--the user may change the table structure without errors,
provided
% the column headers remain relatively consistent
% 3. Does not include functionality to store data, allowing the caller
to
% perform this task as they see fit.

%% PREALLOCATE VARIABLES
t = []; x1 = [];DiffP1=[];Twell1=[];x2=[];DiffP2=[];Twell2=[];BaroP=[];
BattV=[];
```

```
%% DUMP DATA
% You will see the try/catch structure here a lot. Basically it will
*try*
% the commands in the "try" section, and if there is an error, rather
than
% quitting the program outright, it will *catch* the error and instead
% execute the commands in the "catch" section.

if isempty(fn); return;end
FileData = importdata(fn,','); % imports the data from fn into a
                % variable called "FileData";
                % specifies that the columns are
                % separated by commas and that there
                % are four lines in the header.

for i = 1:length(FileData.colheaders)
  hdr = FileData.colheaders{i};
  if strfind(hdr,'TIME')
    t = FileData.data(:,i);
  elseif strfind(hdr,'V1')
    V1 = FileData.data(:,i);
  elseif strfind(hdr,'V2')
    V2 = FileData.data(:,i);
  elseif strfind(hdr,'DataCounts1')
    dc1 = FileData.data(:,i);
  elseif strfind(hdr,'DataCounts2')
    dc2 = FileData.data(:,i);
  elseif strfind(hdr,'DataCounts')
    dc1 = FileData.data(:,i);
  elseif strfind(hdr,'DiffP')
    if strfind(hdr,'2')
      DiffPV2 = FileData.data(:,i);
    else
      DiffPV1 = FileData.data(:,i);
    end
  elseif strfind(hdr,'BaroP')
    BaroP = FileData.data(:,i);
  elseif strfind(hdr,'WellT')
    if strfind(hdr,'1')
      Twell1 = FileData.data(:,i);
    elseif strfind(hdr,'2')
      Twell2 = FileData.data(:,i);
    end
  elseif strfind(hdr,'batt')
    BattV = FileData.data(:,i);
  end
end
%% PROCESS DATA
t = t - 40909;   % This puts the serial date in terms of days since
          % 1/1/12.
%V1 = cts1*2.96e-7;
%V2 = cts2*2.96e-7;
```

```
if exist('dc1','var')
  V1 = dc1*2.96e-7;
end
if exist('V1','var')
  x1 = ConvertDisp(V1); % The function "ConvertDisp" converts the
displacement
          % voltage signal to microns.
  x1 = xMirror(x1);   % The function "xMirror" flips the displacement
data
          % so that decreasing displacement indicates compression
          % while increasing displacement indicates extension.
end
if exist('dc2','var')
  V2 = dc2*2.96e-7;
end
if exist('V2','var')
  x2 = ConvertDisp(V2);
  x2 = xMirror(x2);
end


% This code calculates the differential pressure in Pa by shifting the
zero
% differential pressure point based on the input voltage, subtracting
the
% current voltage (in V) from this new mean value to ensure that
% increasing differential pressure means increasing load on the soil,
and
% converting the corrected output voltage to Pa.
if exist('DiffPV1','var')
  DiffP1 = DiffPV1;
end
if exist('DiffP2','var')
  DiffP2 = DiffPV2;
end

if exist('BaroP','var')
  BaroP = 3377*(1.1981*BaroP/10^3+26.002)/10^3;  % This equation
converts the
          % barometric pressure signal from volts to kPa; divided
          % by 10^3 to convert Pa to kPa, BaroP converted from
          % mV to V.
end

if exist('Twell1','var')
  Twell1 = Twell1/10;  % The well temperature output is 10 mV/degree C;
by
          % dividing the millivolt output by this conversion
          % factor, the temperature in degrees C is calculated.
end
if exist('Twell2','var')
  Twell2 = Twell2/10;
end
```

```
end

function [tW, v,vmax,vdir,R,P,totP,RH,WTemp,tT,T] = HOBOdump(Wfn,Tfn)
%% DUMP DATA

% HOBO Weather Station Data
if ~isempty(Wfn);FileData1 = importdata(Wfn,',',1);end

% Atmospheric Temperature Sensor
if ~isempty(Tfn);FileData2 = importdata(Tfn,',',1);end

%% PROCESS DATA
if exist('FileData1','var')
  for i = 1:length(FileData1.colheaders)
    hdr = FileData1.colheaders{i};
    if strfind(hdr,'Time')
      tW = FileData1.data(:,i)-40909; % Days since 1/1/12
    elseif strfind(hdr,'Wind')
      v = FileData1.data(:,i); % [m/s]
    elseif strfind(hdr,'Gusts')
      vmax = FileData1.data(:,i); % [m/s]
    elseif strfind(hdr,'Direction')
      vdir = FileData1.data(:,i); % [degrees azimuth]
    elseif strfind(hdr, 'Radiation')
      R = FileData1.data(:,i); % [W/m^2]
    elseif strfind(hdr,'Precipitation')
      P = FileData1.data(:,i)*.25; % [mm] (was x tips*(1 mm/tip);
                    % correct is 0.25 mm/tip)
    elseif ~isempty((strfind(hdr,'RH/Temp'))) &&
(strcmp(right(hdr,2),'RH'))
      RH = FileData1.data(:,i);
    elseif ~isempty((strfind(hdr,'RH/Temp'))) &&
(strcmp(right(hdr,1),'C'))
      WTemp = FileData1.data(:,i);
    end
  end

  totP = totvect(P);
  P = CalcPRate(tW,P);
end

if ~exist('v','var'); v = []; end
if ~exist('vmax','var'); vmax = []; end
if ~exist('vdir','var'); vdir = []; end
if ~exist('R','var'); R = []; end
if ~exist('P','var'); P = []; end
if ~exist('totP','var'); totP = []; end
if ~exist('RH','var'); RH = []; end
if ~exist('WTemp','var'); WTemp = []; end

if exist('FileData2','var')
```

```
  tT = FileData2.data(:,1)-40909;
  T = FileData2.data(:,2);
else
  tT = [];
  T = [];
end
end

%% DUMP SOIL MOISTURE DATA
function [tSM, SM] = SMdump(fn)
  data = importdata(fn,',',1);

  tSM = data.data(:,1)-40909;
  SM = data.data(:,2:size(data.data,2));
end

%% SUPPLEMENTARY FUNCTIONS
function [micr] = ConvertDisp(V)
% This function converts the displacement signal from volts to microns

micr = zeros(length(V),1);
DC = [-0.253447;.0997436;.000308991;-.00009599;.000223073; ...
  -.0000791913;.0000131945;-.000000827685];

for i = 1:length(V)
  nV = V(i);
  micr(i) =
1000*(DC(1)+DC(2)*nV+DC(3)*nV^2+DC(4)*nV^3+DC(5)*nV^4+DC(6)*nV^5+DC(7)*
nV^6+DC(8)*nV^7)+250;
end
end

function [y] = xMirror(x)
% This function creates a matrix 'y' that is a mirror image of matrix
'x'
% about an x-axis aligned with the first data point in matrix 'x'.
  y = zeros(length(x),1);
  y(1) = x(1);
  for i = 2:length(x)
    y(i) = 2*y(1) - x(i);
  end
end

function [y] = right(varargin)
% Function: right
% Author: Clay Freeman
% Date: 4/24/2012
%
% DESCRIPTION:
% Returns the specified number of characters from the end of a string
% or array.
%
```

```
% INSTRUCTIONS:
% [y] = right(x,n) outputs n values from the right side of x. If x is a
% matrix, the output will be the n columns from the right side of x.
%
% [y] = right(x,n,i) outputs n values starting with the ith value from
the
% right of x. If x is a matrix, the output will be the n columns
starting
% with the ith value of x.

switch nargin
  case 0 | 1
    error 'Two few input arguments.'
  case 2
    x = varargin{1};
    n = varargin{2};
    len = size(x,2);

    if ischar(x)
      y = x((len-(n-1)):len);
    elseif isa(x,'numeric')
      y = x(:,(len-(n-1)):len);
    else
      msg = strcat('The data input is not a valid type; please ',...
        'enter either a character or numeric array.');
      error(msg)
    end
  case 3
    x = varargin{1};
    n = varargin{2};
    shift = varargin{3};
    len = size(x,2);

    if (len-((shift-1)+n))>0
      y = x(:,(len-((shift-1)+n)):(len-shift));
    else
      y = x(:,1:(len-shift));
    end
end
end
```

Appendix D

MATLAB Numerical Integration of the Boussinesq Solution to Estimate Young's Modulus

```
function [E] = IntegrationRegions01(z,w,h,n,nu,CentCoord,N,Load,delta)
% Function: IntegrationRegions
% Author: Clay Freeman
% Date Created: 1/26/12
%
% GENERAL DESCRIPTION
% This function takes an array of loaded rectangular regions, calls
% another function to calculate the contribution to the shear modulus
of
% each loaded region, totals the stress caused by these regions at a
% monitoring point, and converts the final estimate of shear modulus to
% Young's modulus.
%
% BOUSSINESQ'S EQUATION
% delta = u_z(z1) - u_z(z2) = WA/(4*PI*G)[2*(1-nu)/R+z^2/R^3] | z1 ->
z2
% where W*dA is numerically approximated using a series of point loads
% numerically integrated over the area "A." Solving for G gives
% G = WA/(4*PI*delta)*[2*(1-nu)/R+z^2/R^3] | z1 -> z2
% and G is converted to Young's modulus by the equation
% E = 2*G*(1+nu)
%
% INPUTS
% z = depth to centerline of anchors (z(1) = top, z(2) = bottom) [L]
% w = width (radially from well) of loaded region [L]
% h = height (perpendicular to ray originating at well) of loaded
region
% [L]
% n = 1x2 array; 1,1 is divisions across width; 1,2 is divisions across
% height [-]
% nu = the Poisson ratio of the soil. For saprolite, nu is about 0.35
% CentCoord = nx2 array; n,1 is x coord to the center of the nth loaded
% region; n,2 is the y coord to the center of the nth loaded region [L]
% N is the number of occurrences of each loading region. length(N) ==
% size(CentCoord,1).
% Load = the total load applied to the region [m*L/t^2]
% Instances = nx1 array; n,1 is the number of times the nth region
occurs
% [-]
% delta = measured displacement response of the monitoring point [L]
%
% OUTPUTS
% E = Young's Modulus of the material in which the monitoring point
exists
%
```

```
% Check variables
if length(N) ~= size(CentCoord,1)
    error('N is not specified for every loading region')
end

% Initialize arrays and variables
    dx = w/n(1); % x increment is width/number of divisions across
width
    dy = h/n(2); % y increment is height/number of divisions across
height
    dA = dx*dy; % area increment is (x increment)*(y increment)
    P_i = Load*(dA/(w*h)); % load increment is the total
        % load times the fraction of the total area represented by the
        % area increment

    R = zeros(2,1); % dimension the 3D resultant vector
    G = zeros(n(2)+1,n(1)+1,size(CentCoord,1)); % dimension the
incremental
        % shear modulus vector

    for i = 1:size(CentCoord,1)
        % Calculate the x and y coords for the lower corner of the ith
        % load region
        x = (CentCoord(i,1)-w/2):dx:(CentCoord(i,1)+w/2);
        y = (CentCoord(i,2)-h/2):dy:(CentCoord(i,2)+h/2);

        % Calculate the R values and corresponding E values for each
        % element in the ith load region
        for ii = 1:n(2)+1
            for jj = 1:n(1)+1
                R(1) = sqrt(z(1)^2+x(ii)^2+y(jj)^2);
                R(2) = sqrt(z(2)^2+x(ii)^2+y(jj)^2);
                G(ii,jj,i) = N(i)*CalcGContr(z,R,delta,P_i,nu);
            end
        end
    end
    Gs = sum(sum(sum(abs(G)))); % Scalar shear modulus is the sum of
the
        % incremental measurements of G
    E = 2*Gs*(1+nu); % Convert the shear modulus to the Young's modulus
end
function [G] = CalcGContr(z,R,delta,P_i,nu)
    term1 = (2*(1-nu)/R(1)+z(1)^2/R(1)^3);
    term2 = (2*(1-nu)/R(2)+z(2)^2/R(2)^3);
    G = P_i/(4*pi()*delta)*(term1 - term2);
end
```

REFERENCES

Acworth, R.I. and Brain, T. (2008). Calculation of barometric efficiency in shallow piezometers using water levels, atmospheric and earth tide data. *Hydrogeology Journal 16*.

Akinremi, O. O., McGinn, S. M., & Barr, A. G. (1996). Simulation of soil moisture and other components of the hydrological cycle using a water budget approach. *Canadian Journal of Soil Science, 75*.

Albers, B. (2010). Linear elastic wave propagation in unsaturated sands, silts, loams and clays. *Transport in Porous Media, 86*(2).

Anderson, S.A. and LaFronz, N.J. (2007). Rockfill embankment settlement: Sugarloaf Mountain Bridge abutment and Hoover Dam Bypass (US-93). *Transportation Research Record: Journal of the Transportation Research Board, No. 2016*.

Andréassian, V., Perrin, C., & Michel, C. (2004). Impact of imperfect potential evapotranspiration knowledge on the efficiency and parameters of watershed models. *Journal of Hydrology, 286*.

Andréassian, V., Perrin, C., Michel, C., Usart-Sanchez, I., & Lavabre, J. (2001). Impact of imperfect rainfall knowledge on the efficiency and the parameters of watershed models. *Journal of Hydrology, 250*.

Anochikwa, C. I., van der Kamp, G., & Barbour, S. L. (2009). Numerical simulation of observed pore-pressure changes in an aquitard due to changes of total soil moisture, paper presented at GeoHalifax 2009, Halifax, Nova Scotia.

Artan, G. A., Neale, C. M. U., & Tarboton, D. G. (2000). Characteristic length scale of input data in distributed models: Implications for modeling grid size. *Journal of Hydrology, 227*.

Atkinson, S.E., Woods, R.A., and Sivapalan, M. (2002). Climate and landscape controls on water balance model complexity over changing timescales. *Water Resources Research 38*(12).

Aubinet, M., Vesala, T., & Papale, D. (Eds.). (2012). *Eddy covariance: A practical guide to measurement and data analysis*. New York, NY: Springer.

Bardsley, W. E., & Campbell, D. I. (1994). A new method for measuring near-surface moisture budgets in hydrological systems. *Journal of Hydrology, 154*, 245.

Bardsley, W. E., & Campbell, D. I. (2000). Natural geological weighing lysimeters: Calibration tools for satellite and ground surface gravity monitoring of subsurface water-mass change. *Natural Resources Research, 9*(2).

Bardsley, W. E., & Campbell, D. I. (2007). An expression for land surface water storage monitoring using a two-formation geological weighing lysimeter. *Journal of Hydrology, 335*.

Barnett, T. P., Adam, J. C., & Lettenmaier, D. P. (2005). Potential impacts of a warming climate on water availability in snow-dominated regions. *Nature, 438*(17).

Barr, A. G., van der Kamp, G., Schmidt, R., & Black, T. A. (2000). Monitoring the moisture balance of a boreal aspen forest using a deep groundwater piezometer. *Agricultural and Forest Meteorology, 102*, 13.

Bastiaanssen, W. G. M., Molden, D. J., & Makin, I. W. (2000). Remote sensing for irrigated agriculture: Examples from research and possible applications. *Agricultural Water Management, 46*.

Bates, B., Kundzevicz, Z. W., Wu, S., & Palutikof, J. (Eds.). (2008). *Climate change and water*. IPCC Secretariat, Geneva: Technical Paper of the Intergovernmental Panel on Climate Change.

Bell, V.A., Kay, A.L., Jones, R.G., Moore, R.J., and Reynard, N.S. (2009). Use of soil data in a grid-based hydrological model to estimate spatial variation in changing flood risk across the UK. *Journal of Hydrology 377*.

Bemer, E., Longuemare, P., and Vincké, O. (2004). Poroelastic parameters of Meuse/Haute Marne argillites: effect of loading and saturation states. *Applied Clay Science 26.*

Berg, S. J., Hsieh, P. A., & Illman, W. A. (2011). Estimating hydraulic parameters when poroelastic effects are significant. *Ground Water, 49*(6).

Berryman, J. G. (2011). Mechanics of layered anisotropic poroelastic media with applications to effective stress for fluid permeability. *International Journal of Engineering Science, 49*.

Bjerklie, D.M., Trombley, T.J., and Viger, R.J. (2011). Simulations of historical and future trends in snowfall and groundwater recharge for basins draining to Long Island Sound. *Earth Interactions 15.*

Bohnenstengel, S. I., Schlunzen, K. H., & Beyrich, F. (2011). Representativity of *in situ* precipitation measurements – A case study for the LITFASS area in north-eastern Germany. *Journal of Hydrology, 400*.

Boussinesq, J.Équilibre élastique d'un solide isotrope de masse négligeable, soumis à différents [elastic equilibrium of a weightless isotropic solid under various loads] . *C. Rend. Acad. Sci. Paris, 86*, 1260.

Boutt, D. F. (2010). Poroelastic loading of an aquifer due to upstream dam releases. *Ground Water, 48*(4).

Brocca, L., Melone, F., Moramarco, T., and Morbidelli, R. (2010). Spatial-temporal variability of soil moisture and its estimation across scales. *Water Resources Research 46*.

Burbey, T. J., Hisz, D., Murdoch, L. C., & Zhang, M. (2012). Quantifying fractured crystalline-rock properties using well tests, earth tides and barometric effects. *Journal of Hydrology, 414-415*.

Butler, J., Jr., Kluitenberg, G. J., Whittemore, D. O., Loheide, S. P., II, Jin, W., Billinger, M. A., & Zhan, X. (2007). A field investigation of phreatophyte-induced fluctuations in the water table. *Water Resources Research, 43*.

Chen, J., Chen, W., Liu, J., & Cihlar, J. (2000). Annual carbon balance of Canada's forests during 1895-1996. *Global Biogeochemical Cycles, 14*(3).

Cooper, R., Hodgkins, R., Wadham, J., & Tranter, M. (2011). The hydrology of the proglacial zone of a high-arctic glacier(Finsterwalderbreen, Svalbard): Sub-surface water fluxes and complete water budget. *Journal of Hydrology, 406*.

Crow, W. T., Ryu, D., & Famiglietti, J. S. (2005). Upscaling of field-scale soil moisture measurements using distributed land surface modeling. *Advances in Water Resources, 28*.

Czikowsky, M. J., & Fitzjarrald, D. R. (2009). Detecting rainfall interception in an Amazonian rain forest with eddy flux measurements. *Journal of Hydrology, 377*.

Daniel, III., C.C. and Harned, D.A. (1998). Ground-water recharge to and storage in the regolith-fractured crystalline rock aquifer system, Guilford County, North Carolina. U.S. Geological Survey. Water-Resources Investigations Report 97-4140.

Das, B.M. (2006). *Principles of Geotechnical Engineering* (6th ed.). Toronto, Ontario, Canada: Nelson.

Davis, R.O. and Selvadurai, A.P.S. (1996). *Elasticity and Geomechanics*. Cambridge, UK: Cambridge University Press.

Delahaye, J., Gole´, P., & Waldteufel, P. (2002). Calibration error of L-band sky-looking ground-based radiometers. *Radio Science, 37*(1).

Delwart, S., Bouzinac, C., Wursteisen, P., Berger, M., Drinkwater, M., Martín-Neira, M., & Kerr, Y. H. (2008). SMOS validation and the COSMOS campaigns. *IEEE Transactions on Geoscience and Remote Sensing, 46*(3).

Dennehy, K.F., Litke, D.W., and McMahon, P.B. (2002). The High Plains Aquifer, USA; groundwater development and sustainability. *Geological Society Special Publications 193*.

Desilets, D., Zreda, M., & Ferré, T. P. A. (2010). Nature's neutron probe: Land surface hydrology at an elusive scale with cosmic rays. *Water Resources Research, 46*.

Detournay, E., & Cheng, A. H. -. (1993). Fundamentals of poroelasticity. In C. Fairhurst (Ed.), *Comprehensive rock engineering*.

Dinesh, S. V., Yamada, S., & Hyodo, M. (2008). Low strain shear modulus of sand-clay mixtures. New Orleans, LA. *, 178*.

Dolph, J., D. Marks, and G. A. King. 1991. Sensitivity of the regional water balance in the Columbia River basin to climate variability: Application of a spatially distributed water balance model. In *New perspectives for watershed management: Balancing Long-Term Sustainability with Cumulative Environmental Change*, (R. J. Naiman and J.R. Sedell, eds.)

Entekhabi, D., Njoku, E. G., Houser, P., Spencer, M., Doiron, T., Kim, Y., & van Zyl, J. (2004). The hydrosphere state (HYDROS) satellite mission: An earth system pathfinder for global mapping of soil moisture and land freeze/thaw *IEEE Transactions on Geoscience and Remote Sensing,42*(10).

Famiglietti, J. S., Devereaux, J. A., Laymon, C. A., Tsegaye, T., Houser, P. R., Jackson, T. J., and van Oevelen, P. J. (1999). Ground-based investigation of soil moisture variability within remote sensing footprints during the southern great plains 1997 (SGP97) hydrology experiment. *Water Resources Research, 35*(6).

Famiglietti, J. S., Ryu, D., Berg, A. A., Rodell, M., & Jackson, T. J. (2008). Field observations of soil moisture variability across scales. *Water Resources Research, 44*.

Farrell, W. E. (1972). Deformation of the earth by surface loads. *Reviews of Geophysics and Space Physics, 10*(3).

Fischer, A. P. (2011). The measurement factors in estimating snowfall derived from snow cover surfaces using acoustic snow depth sensors. *Journal of Applied Meteorology and Climatology, 50*.

Galagedara, L.W., Parkin, G.W., Redman, J.D., von Bertoldi, P., and Endres, A.L. (2005). Field studies of the GPR ground wave method for estimating soil water content during irrigation and drainage. *Journal of Hydrology 301*.

Gallego-Elvira, B., Baille, A., Martín-Gorriz, B., Maestre-Valero, J. F., & Martínez-Alvarez, V. (2012). Evaluation of evaporation estimation methods for a covered reservoir in a semi-arid climate (south-eastern Spain). *Journal of Hydrology, 458-459*.

Galloway, D., Jones, D.R., and Ingebritsen, S.E. (1999). Land subsidence in the United States. U.S. Geological Survey Circular 1182. Reston, VA.

Gao, H., Tang, Q., Ferguson, C. R., Wood, E. F., & Lettenmaier, D. P. (2010). Estimating the water budget of major US river basins via remote sensing. *International Journal of Remote Sensing, 31*(14).

Grant, D. R. (1975). Comparison of evaporation measurements using different methods. *Quarterly Journal of the Royal Meteorological Society, 101*(429).

Grote, K., Hubbard, S., and Rubin, Y. (2003). Field-scale estimation of volumetric water content using ground-penetrating radar ground wave techniques. *Water Resources Research 39*(11).

Gupta, P.K., Oza, S.R., and Panigrahy, S. (2011). Monitoring transplanting operation of rice crop using passive microwave radiometer data. *Biosystems Engineering 108.*

Gurdak, J. J., Hanson, R. T., & Green, T. R. (2009). *Effects of climate variability and change on groundwater resources of the united states.* U.S. Geological Survey Fact Sheet 2009-3074.

Hantel, M., & Acs, F. (1998). Physical aspects of the weather generator. *Journal of Hydrology, 212-213*.

Hargreaves, G. H. (1974). Estimation of potential and crop evapotranspiration. *TRANSACTIONS of the ASAE, 17*(4).

Hefner, B. T., & Jackson, D. R. (2010). Dispersion and attenuation due to scattering from heterogeneities of the frame bulk modulus of a poroelastic medium. *Journal of the Acoustical Society of America, 127*(6).

Hibbeler, R. C. (Ed.). (2005). *Mechanics of materials* (6th ed.). Upper Saddle River, NJ: Pearson Prentice Hall.

Holmes, J. W. (1984). Measuring evapotranspiration by hydrological methods. *Agricultural Water Management, 8*.

Hsu, K., Yeh, H., Chen, Y., Lee, C., Wang, C., & Chiu, F. (2012). Basin-scale groundwater response to precipitation variation and anthropogenic pumping in Chih-Ben watershed, Taiwan. *Hydrogeology Journal, 20*.

Hwang, T., Band, L, and Hales, T.C. (2009). Ecosystem processes at the watershed scale: extending optimality theory from plot to catchment. *Water Resources Research 45*.

Iwata, T., Urabe, J., and Mitsuhashi, H. (2010). Effects of drainage-basin geomorphology on insectivorous bird abundance in temperate forests. *Conservation Biology 24*(5).

Jacobs, J. M., Myers, D. A., Anderson, M. C., & Diak, G. R. (2000). GOES surface insolation to estimate wetlands evapotranspiration. *Journal of Hydrology, 266*.

Kannan, N., Santhi, C., Williams, J. R., & Arnolod, J. G. (2008). Development of a continuous soil moisture accounting procedure for curve number methodology and its behavior with different evapotranspiration methods. *Hydrological Processes, 22*.

Kerr, Y. (1998). SMOS-MIRAS on RAMSES: Radiometry applied to soil moisture and salinity measurements, full proposal, A.O. Earth Explorer Opportunity Missions, European Space Agency, Paris.

Kihm, J., Kim, J., Song, S., & Lee, G. (2007). Three-dimensional numerical simulation of fully coupled groundwater flow and land deformation due to groundwater pumping in an unsaturated fluvial aquifer system. *Journal of Hydrology, 335*.

Kim, J. (2000). Generalized poroelastic analytical solutions for pore water pressure change and land subsidence due to surface loading. *Geosciences Journal, 4*(2).

Kirtland, B. C., Aelion, C. M., & Widdowson, M. A. (2001). Long-term AS/SVE for petroleum removal in low-permeability piedmont saprolite. *Journal of Environmental Engineering, 134*.

Kodama, M., Kudo, S., and Kosuge, T. (1985). Application of atmospheric neutrons to soil moisture measurement. *Soil Science 140*(4).

Korpela, I., Koskinen, M., Vasander, H., Holopainen, M. and Minkkinen, K. (2009). Airborne small-footprint discrete-return LiDAR data in the assessment of boreal mire surface patterns, vegetation, and habitats. *Forest Ecology and Management 258*.

Kurum, M., Lang, R.H., O'Neill, P.E., Joseph, A.T., Jackson, T.J., and Cosh, M.H. (2009). L-band radar estimation of forest attenuation for active/passive soil moisture inversion. *IEEE Transactions on Geoscience and Remote Sensing 47*(9).

Legates, D. R., & Willmott, C. J. (1990). Mean seasonal and spatial variability in gauge-corrected, global precipitation. *International Journal of Climatology, 10*.

Lemaître, F., Poussière, J., Kerr, Y. H., Déjus, M., Durbe, R., de Rosnay, P., & Calvet, J. (2004). Design and test of the ground-based L-Band Radiometer for estimating water in soils (LEWIS). *IEEE Transactions on Geoscience and Remote Sensing, 42*(8).

Lettenmaier, D. P., Brettmann, K. L., Vail, L. W., Yabusaki, S. B., and Scott, M. J. (1992). Sensitivity of Pacific Northwest water resources to global warming. *The Northwest Environmental Journal 8*.

Li, R., Zhu, A., Song, X., Li, B., Pei, T., & Qin, C. (2012). Effects of spatial aggregation of soil spatial information on watershed hydrological modelling. *Hydrological Processes, 26*.

Lopatnikov, S. L., & Gillespie Jr., J. W. (2010). Poroelasticity-I: Governing equations of the mechanics of fluid-saturated porous materials. *Transport in Porous Media, 84*.

Lundberg, A. (1993). Evaporation of intercepted snow—review of existing and new measurement methods. *Journal of Hydrology, 151*.

Malek, E., & Bingham, G. E. (1993). Comparison of the bowen ratio-energy balance and the water balance methods for the measurement of evapotranspiration. *Journal of Hydrology, 146*.

Marin, S., van der Kamp, G., Pietroniro, A., Davison, B., & Toth, B. (2010). Use of geological weighing lysimeters to calibrate a distributed hydrological model for the simulation of land-atmosphere moisture exchange. *Journal of Hydrology, 383*, 179.

Marks, D., King, G. A., and J. Dolph. (1993). Implications of climate change for the water balance of the Columbia River Basin, USA. *Climate Research 2*.

Markstrom, S.L., Hay, L.E., Ward-Garrison, C.D., Risley, J.C., Battaglin, W.A., Bjerklie, D.M., … and Walker, J.F. (2012). Integrated watershed-scale response to climate change for selected basins across the United States. U.S. Geological Survey Scientific Investigations Report 2011-5077. Reston, VA.

McMaster-Carr (2011). More about hard fiber, fiberglass, garolite, and carbon fiber. Retrieved from: http://www.mcmaster.com/#8549kac/=k7i7mj.

Milewski, A., Sultan, M., Yan, E., Becker, R., Abdeldayem, A., Soliman, F., & Gelil, K. A. (2009). A remote sensing solution for estimating runoff and recharge in arid environments. *Journal of Hydrology, 373*.

Murdoch, L.C., Richardson, J.R., Tan, Q., Malin, S.C., and Fairbanks, C. (2006). Forms and sand transport in shallow hydraulic fractures in residual soil. *Canadian Geotechnical Journal 43*.

Ng, C. W. W., & Leung, E. H. Y. (2007). Small-strain stiffness of granitic and volcanic saprolites in Hong Kong. *Characterisation and Engineering Properties of Natural Soils,* Singapore.

Njoku, E.G. and Entekhabi, D. (1996). Passive microwave remote sensing of soil moisture. *Journal of Hydrology 184*.

Oudin, L., Perrin, C., Mathevet, T., Andréassian, V., & Michel, C. (2006). Impact of biased and randomly corrupted inputs on the efficiency and the parameters of watershed models. *Journal of Hydrology, 320*.

Palmer, M.A., Lettenmaier, D.P., Poff, N.L., Postel, S.L., Richter, B., and Warner, R. (2009). Climate change and river ecosystems: protection and adaptation options. *Environmental Management 44*.

Parsons, L.R. and Bandaranayake, W.M. (2009). Performance of a new capacitance soil moisture probe in a sandy soil. *Soil Science Society of America Journal 73*(4).

Penman, H. L. (1948). Natural evaporation from open water, bare soil and grass. *Proceedings of the Royal Society of London A, 193*(1032).

Peterson, T. C., Easterling, D. R., Karl, T. R., & Groisman, P. (1998). Homogeneity adjustments of *in situ* atmospheric climate data: A review. *International Journal of Climatology, 18*.

Peterson, T. C., Easterling, D. R., Karl, T. R., Groisman, P., Nicholls, N., Plummer, N., and Parker, D. (1998). Homogeneity adjustments of *in situ* atmospheric climate data: a review. *International Journal of Climatology, 18*.

Purvis, J.C. (2010). Pan evaporation records for the South Carolina area. South Carolina State Climatology Office. Retrieved from http://www.dnr.sc.gov/climate/sco/Publications/pan_evap_records.php.

Ratnam, S., Soga, K., & Whittle, R. W. (2005). A field permeability measurement technique using a conventional self-boring pressuremeter. *Géotechnique, 55*(7).

Robinson, D. A., Campbell, C. S., Hopmans, J. W., Hornbuckle, B. K., Jones, S. B., Knight, R., and Wendroth, O. (2008). Soil moisture measurement for ecological and hydrological watershed-scale observatories: A review. *Vadose Zone Journal, 7*(1).

Rojstaczer, S. (1988). Determination of fluid flow properties from the response of water levels in wells to atmospheric loading. *Water Resources Research, 24*(11).

Rojstaczer, S. (1989). The influence of formation material properties on the response of water levels in wells to earth tides and atmospheric loading. *Journal of Geophysical Research, 94*(B9).

Ruiz, L., Varma, M.R., Kumar, M.S., Sekhar, M., Maréchal, J., Descloitres, M., … and Braun, J. (2010). Water balance modelling in a tropical watershed under deciduous forest (Mule Hole, India): regolith matric storage buffers the groundwater recharge process. *Journal of Hydrology 380*.

Saleh, K., Wigneron, J.-P., Waldteufel, P., de Rosnay, P., Schwank, M., Calvet, J.-C., and Kerr, Y.H., (2007). Estimates of surface soil moisture under grass covers using L-band radiometry. *Remote Sensing of Environment 109.*

Saleh, K., Kerr, Y.H., Richaume, P., Escorihuela, M.J., Panciera, R., Delwart, S., … and Wigneron, J.P. (2009). Soil moisture retrievals at l-band using a two-step inversion approach (COSMOS/NAFE'05 experiment). *Remote Sensing of Environment 113*.

Schoeneberger, P., & Amoozegar, A. (1990). Directional saturated hydraulic conductivity and macropore morphology of a soil-saprolite sequence. *Geoderma, 46*.

Schweisinger, T., Murdoch, L., & Huey Jr., C. (2007). Removable borehole extensometers for measuring axial displacements during well tests. *Geomechanical Testing Journal, 30*(3).

Schweisinger, T., Svenson, E. J., & Murdoch, L. C. (2009). Introduction to hydromechanical well tests in fractured rock aquifers. *Ground Water, 47*(1).

Schweisinger, T., Svenson, E. J., & Murdoch, L. C. (2011). Hydromechanical behavior during constant-rate pumping tests in fractured gneiss. *Hydrogeology Journal, 19*.

Sharma, M.L. (1986). Measurement and prediction of natural groundwater recharge – an overview. *Journal of Hydrology 25*(1).

Shuttleworth, W. J. (2008, Evapotranspiration measurement methods. *Southwest Hydrology, 23*.

Smerdon, B.D., Allen, D.M., Grasby, S.E., and Berg, M.A. (2009). An approach for predicting groundwater recharge in mountainous watersheds. *Journal of Hydrology 265*.

Sophocleous, M., Bardsley, E., & Healey, J. (2006). A rainfall loading response recorded at 300 meters depth: Implications for geological weighing lysimeters. *Journal of Hydrology, 319*.

Sulis, M., Paniconi, C., & Camporese, M. (2011). Impact of grid resolution on the integrated and distributed response of a coupled surface–subsurface hydrological model for the des Anglais catchment, Quebec. *Hydrological Processes, 25*.

Svenson, E. J., Schweisinger, T., & Murdoch, L. C. (2007). Analysis of the hydromechanical behavior of a flat-lying fracture during a slug test. *Journal of Hydrology, 347*.

Svenson, E. J., Schweisinger, T., & Murdoch, L. C. (2008). Field evaluation of the hydromechanical behavior of flat-lying fractures during slug tests. *Journal of Hydrology, 359*.

Swenson, S., & Wahr, J. (2006). Estimating large-scale precipitation minus evapotranspiration from GRACE satellite gravity measurements. *Journal of Hydrometeorology, 7*.

Tenenbaum, D.E., Band, L.E., Kenworthy, S.T., and Tague, C.L. (2006). Analysis of soil moisture patterns in forested and suburban catchments in Baltimore, Maryland, using high-resolution photogrammetric and LIDAR digital elevation datasets. *Hydrological Processes 20*.

Thoma, D.P., Moran, M.S., Bryant, R., Rahman, M.M., Holifield Collins, C.D., Keefer, T.O., … and Peters-Lidard, C.D. (2008). Appropriate scale of soil moisture retrieval from high resolution radar imagery for bare and minimally vegetated soils. *Remote Sensing of Environment 112*.

Thornthwaite, C. W., (1948). An approach toward a rational classification of climate, *Geographical Review, 38*(1).

USDA Web Soil Survey, 2012 (2012). Retrieved from: http://websoilsurvey.nrcs.usda.gov/app/HomePage.htm.

van der Kamp, G., & Gale, J. E. (1983). Theory of earth tide and barometric effects in porous formations with compressible grains. *Water Resources Research, 19*(2), 538.

van der Kamp, G., & Maathuis, H. (1991). Annual fluctuations of groundwater levels as a result of loading by surface moisture. *Journal of Hydrology, 127*.

van der Kamp, G., & Schmidt, R. (1997). Monitoring of total soil moisture on a scale of hectares using groundwater piezometers. *Geophysical Research Letters, 24*(6), 719.

van Overmeeren, R.A., Sariowan, S.V., and Gehrels, J.C. (1997). Ground penetrating radar for determining volumetric soil water content; results of comparative measurements at two test sites. *Journal of Hydrology 197*.

Vellidis, G., Smith, M.C., Thomas, D.L., and Asmussen, L.E. (1990). Detecting wetting front movement in a sandy soil with ground-penetrating radar. *Transactions of the ASAE 33*(6).

Wahr, J., & Molenaar, M. (1998). Time variability of the Earth's gravity field: Hydrological and oceanic effects and their possible detection using GRACE. *Journal of Geophysical Research, 103*.

Wang, S., & Hsu, K. (2009). Dynamics of deformation and water flow in heterogeneous porous media and its impact on soil properties. *Hydrological Processes, 23*.

Western, A.W. and Blöschl, G. (1999). On the spatial scaling of soil moisture. *Journal of Hydrology 217*.

Wisely, B. A., & Schmidt, D. (2010). Deciphering vertical deformation and poroelastic parameters in a tectonically active fault-bound aquifer using InSAR and well level data, san Bernardino basin, California. *Geophysical Journal International, 181*.

Wong, C.S. (1978). Atmospheric input of carbon dioxide from burning wood. *Science 200*.

Yatheendradas, S., Wagener, T. Gupta, H., Unkrich, C., Goodrich, D., Schaffner, M., and Steward, A. (2008). Understanding uncertainty in distributed flash flood forecasting for semiarid regions. *Water Resources Reseasrch 44*.

Zreda, M., Desilets, D., Ferré, T. P. A., & Scott, R. L. (2008). Measuring soil moisture content non-invasively at intermediate spatial scale using cosmic-ray neutrons. *Geophysical Research Letters, 35*.

Zreda, M., Shuttleworth, W. J., Zeng, X., Zweck, C., Desilets, D., Franz, T., Ferré, T. P. A. (2012). COSMOS: The COsmic-ray Soil Moisture Observing System. *Hydrology and Earth System Sciences Discussions, 9*.